Standard multiscale entropy reflects spectral power at mismatched temporal scales: What's signal irregularity got to do with it?

Short title: Multi-scale entropy reflects spectral power

Julian Q. Kosciessa[123]*, Niels A. Kloosterman[12], and Douglas D. Garrett[12]*

[1]Max Planck UCL Centre for Computational Psychiatry and Ageing Research, Berlin, Germany

[2]Center for Lifespan Psychology, Max Planck Institute for Human Development, Berlin, Germany

[3]Department of Psychology, Humboldt-Universität zu Berlin, Berlin, Germany

* Corresponding authors: kosciessa@mpib-berlin.mpg.de; garrett@mpib-berlin.mpg.de

Author ORCIDs

Julian Q. Kosciessa – http://orcid.org/0000-0002-1134-7996
Niels A. Kloosterman – http://orcid.org/0000-0002-1134-7996
Douglas D. Garrett – https://orcid.org/0000-0002-0629-7672

Keywords

multiscale sample entropy; irregularity; resting state EEG; age differences; rhythms

Abstract

Multiscale Entropy (MSE) is increasingly used to characterize the temporal irregularity of neural time series patterns. Due to its' presumed sensitivity to non-linear signal characteristics, MSE is typically considered a complementary measure of brain dynamics to signal variance and spectral power. However, the divergence between these measures is often unclear in application. Furthermore, it is commonly assumed (yet sparingly verified) that entropy estimated at specific time scales reflects signal irregularity at those precise time scales of brain function. We argue that such assumptions are not tenable. Using simulated and empirical electroencephalogram (EEG) data from 47 younger and 52 older adults, we indicate strong and previously underappreciated associations between MSE and spectral power, and highlight how these links preclude traditional interpretations of MSE time scales. Specifically, we show that the typical definition of temporal patterns via "similarity bounds" biases coarse MSE scales – that are thought to reflect slow dynamics – by high-frequency power. Moreover, we demonstrate that entropy at fine time scales – presumed to indicate fast dynamics – is highly sensitive to broadband spectral power, a measure dominated by low-frequency contributions. Jointly, these issues produce counterintuitive reflections of frequency-specific content on MSE time scales. We emphasize the resulting inferential problems in a conceptual replication of cross-sectional age differences at rest, in which scale-specific entropy age effects could be explained by spectral power differences at mismatched temporal scales. Furthermore, we demonstrate how such problems may be alleviated, resulting in the indication of scale-specific age differences in rhythmic irregularity. Finally, we recommend best practices that may better permit a valid estimation and interpretation of neural signal irregularity at time scales of interest.

Author Summary

Brain signals exhibit a wealth of dynamic patterns that that are thought to reflect ongoing neural computations. Multiscale sample entropy (MSE) intends to describe the temporal irregularity of such patterns at multiple time scales of brain function. However, the notion of time scales may often be unintuitive. In particular, traditional implementations of MSE are sensitive to slow fluctuations at fine time scales, and fast dynamics at coarse time scales. This conceptual divergence is often overlooked and may lead to difficulties in establishing the unique contribution of MSE to effects of interest over more established spectral power. Using simulations and empirical data, we highlight these issues and provide evidence for their relevance for valid practical inferences. We further highlight that standard MSE and traditional spectral power are highly collinear in our example. Finally, our analyses indicate that spectral filtering can be used to estimate temporal signal irregularity at matching and intuitive time scales. To guide future studies, we make multiple recommendations based on our observations. We believe that following these suggestions may advance our understanding of the unique contributions of neural signal irregularity to neural and cognitive function across the lifespan.

Introduction

Entropy as a measure of signal irregularity

Neural times series exhibit a wealth of dynamic patterns that are thought to reflect ongoing neural computations. While some of these patterns consist of stereotypical deflections [e.g., periodic neural rhythms; 1, 2], the framework of nonlinear dynamics and complex systems increasingly emphasizes the importance of temporal irregularity (or variability) for healthy, efficient, and flexible neural function [3-6]. In parallel with such conceptual advances, multiscale entropy (MSE) [7, 8], an information-theoretic index that estimates sample entropy [9] at multiple time scales (Fig 1A), is increasingly applied to quantify the irregularity of neural time series across different brain states, the lifespan, and in relation to health and disease [10-18].

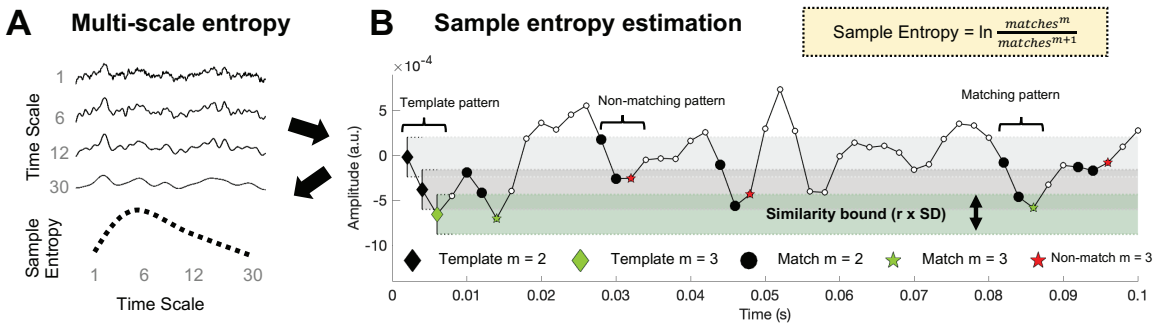

Fig 1. Traditional MSE estimation procedure. (**A**) Multi-scale entropy is an extension of sample entropy, an information-theoretic metric intended to describe the temporal irregularity of time series data. To estimate entropy for different time scales, the original signal is traditionally 'coarse-grained' using low-pass filters, followed by the calculation of the sample entropy. (**B**) Sample entropy estimation procedure. Sample entropy measures the conditional probability that two amplitude patterns of sequence length m (here, 2) remain similar (or matching) when the next sample ***m*** + 1 is included in the sequence. Hence, sample entropy increases with temporal irregularity, i.e., with the number of m-length patterns that do not remain similar at length m+1 (non-matches). To discretize temporal patterns from continuous amplitudes, similarity bounds (defined as a proportion ***r,*** *here .5,* of the signal variance) define amplitude ranges around each sample in a given template sequence, within which matching samples are identified in the rest of the time series. These are indicated by horizontal grey and green bars around the first three template samples. This procedure is applied to each template sequence in time, and the pattern counts are summed to estimate the signal's entropy. The exemplary time series is a selected empirical EEG signal that was 40-Hz high-pass filtered with a 6th order Butterworth filter.

In general, sample entropy quantifies the irregularity of temporal patterns in a given signal (for an example of its calculation, see Fig 1B). Whereas signals with a repetitive structure (like stationary signals or rhythmic fluctuations) are estimated as having low entropy, less predictable (or random) signals are ascribed high entropy. As an extension of this principle, MSE aims to describe temporal irregularity at different time scales – varying from fine (also referred to as 'short') to coarse (or 'long'). In conventional Fourier analysis of time series data, time scales are quantified in terms of lower and higher frequencies present in the signal. This has been shown to be a principled time scale descriptor that relates at least in part to structural properties of the generating neural circuits [2, 19-22]. Given this meaningful definition of fast and slow events, it is a common assumption – including in guides to MSE's interpretation in

neural applications [23] – that fine-to-coarse scales characterize the irregularity of high-to-low frequency dynamics, respectively. However, here we identify one methodological and one conceptual issue regarding the computation of MSE that challenge such a direct scale-to-frequency mapping. First, we first show that the traditional definition of temporal patterns may lead to an influence of high frequencies on coarse entropy time scales (Issue 1). Second, we establish that the signal content at fine time scales renders entropy estimates sensitive to slow fluctuations (Issue 2).

Due to its assessment of temporal patterns rather than oscillatory dynamics, MSE has been motivated as a complementary measure to spectral variance/power that is sensitive to non-linear signal characteristics, such as phase shifts or cross-frequency coupling. [Note that we use the terms power and variance interchangeably, as a time domain signal's broadband variance is proportional to the integral of its power spectral density, while narrowband variance in the time domain is identical to narrowband power in the spectral domain.] However, the overlap between these measures is often unclear in application because the mapping between spectral power and scale-wise entropy is ambiguous. Such ambiguity affects both the ability to compare individuals at any scale, and the ability to compare entropy levels across scales within person. We argue that a clarification of these issues is thus necessary for valid inferences of time scale-specific 'neural irregularity' in a growing number of neuroscientific MSE applications.

Issue 1: Global similarity bounds introduce a scale-dependent variance bias

A principle assumption of sample entropy is that "the degree of irregularity of a complex signal […] cannot be entirely captured by the SD [i.e., standard deviation]" [24; i.e., square root of variance]. To ensure this, sample entropy is typically assessed relative to the standard deviation of the broadband signal to intuitively normalize the estimation of irregularity for overall distributional width [9, 10, see also 24]. In particular, the ***similarity bound*** – defined by a constant r, by which the signal SD is multiplied – reflects the tolerance for labeling time points as being similar or different, and thus, determines how liberal the algorithm is towards detecting 'matching patterns' (Fig 2A-C). While wider bounds decrease entropy estimates, narrower bounds increase them [9, 25, 26] (S2 Figure). Crucially, the similarity bound is often not equally liberal across time scales, resulting in an entropy estimation bias. Specifically, to characterize temporal irregularity at coarser time scales, signals are typically successively low-pass filtered [or 'coarse-grained'; 27] (Fig 2D), whereas the similarity bound typically (in its 'Original' implementation) is set only once – namely relative to the SD of the original unfiltered signal. Due to the progressive filtering, coarse-graining successively removes variance from the signal, yet a single global (i.e., scale-invariant) similarity bound remains based on the cumulative variance of all estimable frequencies (Fig 2D and E). As a result, the similarity bound becomes increasingly liberal towards pattern similarity at coarser scales, thereby reducing entropy estimates. This is most clearly illustrated by the observation that white noise signals, which should be characterized as equally random at each time scale, exhibit decreasing entropy values towards coarser scales when global *similarity bound*s are used [23, 25, 28]. This issue has been recognized previously [25], and provided a rationale for recomputing the *similarity bound* for each time scale [25, 29]. But despite the benefits of this refinement that was already proposed fifteen years ago, our review of the literature revealed that the use of global bounds remains

dominant in over 90% of neuroscientific MSE applications (see S1 File) and in previous validation work [23]. Thus, we argue that a comprehensive assessment of the resulting bias is needed to highlight this issue, both to clarify previous results and to guide future studies.

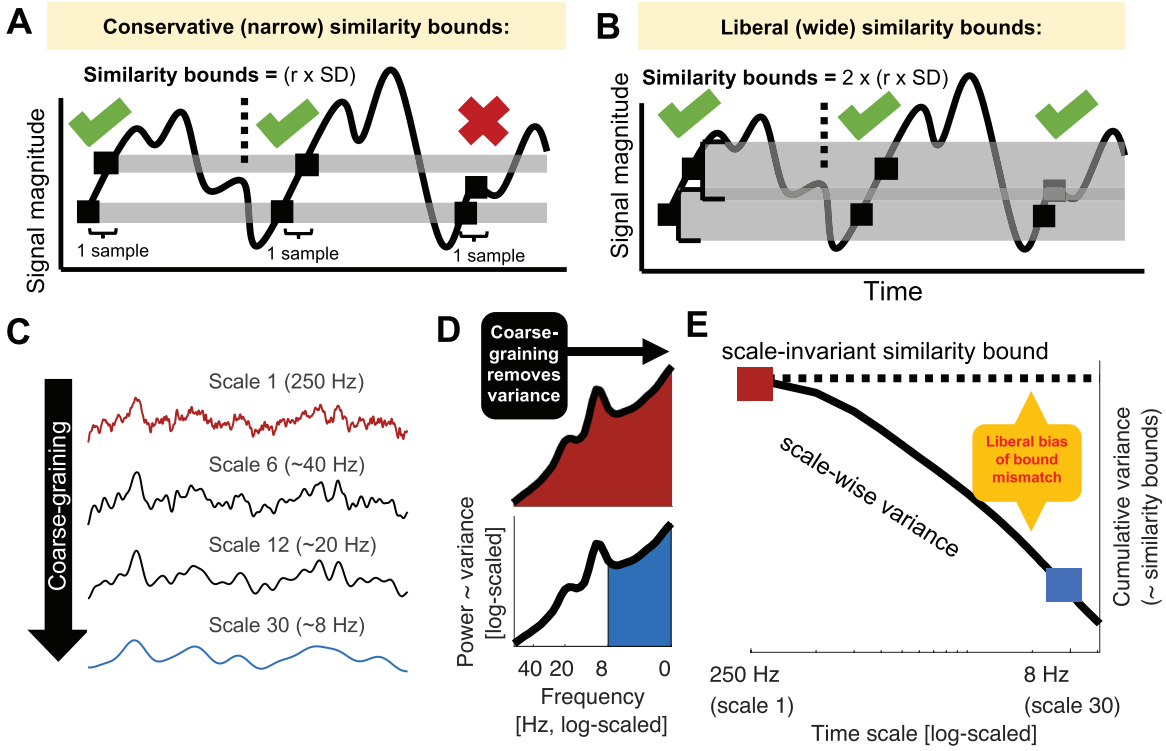

Fig 2. Issue 1: Global similarity bounds systematically confound the entropy of coarse-scale signals with removed spectral power. (**A, B**) Similarity bounds constrain sample entropy as shown schematically for entropy estimation using narrower (**A**) and wider (**B**) similarity bounds. For clarity, only a subset of pattern matches (green ticks) and mismatches (red cross) are indicated for a sequence length m = 1(cf. Fig 1B). Wider, more liberal similarity bounds indicate more pattern matches than narrow, conservative bounds, thereby decreasing entropy. S2 Figure shows the empirical link between liberal similarity bounds and sample entropy estimates. (**C-E**) Divergence between global similarity bounds and scale-wise signal SD biases coarse-scale entropy. (**C**) Coarse-graining (see Figure 1A) progressively reduces variance from the original broadband signal (as shown in panel E). (**D**) At original sampling rates (i.e., time scale 1; marked red in panels DE and F), neural signal variance is usually composed of broadband 1/f content and narrowband rhythmic peaks. Note that the x-axis plots decreasing frequencies to align with the traditional MSE low-pass filter direction. Towards coarser scales (e.g., scale 30; marked blue in CD and E), signal variance progressively decreases, as the signal becomes more specific to low frequencies. (**E**) Due to the systematic and cumulative reduction of variance in scale-wise signals, global similarity bounds become liberally biased ('broad'). Critically, systematic differences in the magnitude of this bias (e.g., due to different spectral slopes) introduce systematic entropy differences at coarser scales.

Issue 2: Traditional scale definitions lead to diffuse time scale reflections of spectral content

While matched similarity bounds account for *total signal variation* at any specific time scale, sample entropy remains related to *the variance structure* (i.e., the power spectrum) of the signal as ***one*** indicator of its temporal irregularity [4]. Most neural signals exhibit a scale-free $\frac{1}{f^x}$ power distribution [30, 31], for which the exponent x indicates the prevalence of low-to-high-frequency components in the signal. This ratio is also referred to as the power spectral

density (PSD) slope. Smaller exponents (indicating shallower PSD slopes) characterize signals with relatively strong high-frequency contributions (i.e., reduced temporal autocorrelations, and less predictability) compared to larger exponents indicating steeper slopes. This conceptual link between PSD slopes and sample entropy has been empirically observed both across subjects and wakefulness states [10, 13, 32]. However, the sensitivity of fine-scale entropy to PSD slopes – a multi-scale characteristic – highlights that the contribution of slow-to-fast signal content to fine-scale entropy is unclear. This ambiguity arises from the algorithm that derives scale-wise signals. In particular, 'Original' MSE implementations use low-pass filters to derive signals at coarser time scales, which increasingly constrains entropy estimates to slower fluctuations. However, the opposite is not true. Hence, finer time scales characterize the *entire* broadband signal (see Fig 3A) which represents a non-specific mixture of both low and high frequency elements [33, 34]. Crucially, the contribution of these elements to neural broadband signals is not equal. Rather, the variance of $\frac{1}{f^x}$ signals is dominated by the amplitude of low frequencies, which may thus disproportionally impact the assessment of pattern irregularity. As a result, broadband signal characterization challenges the assumption that fine-scale entropy mainly describes 'fast' events. More generally, this highlights large uncertainty regarding the frequencies that are represented at *any* particular time scale.

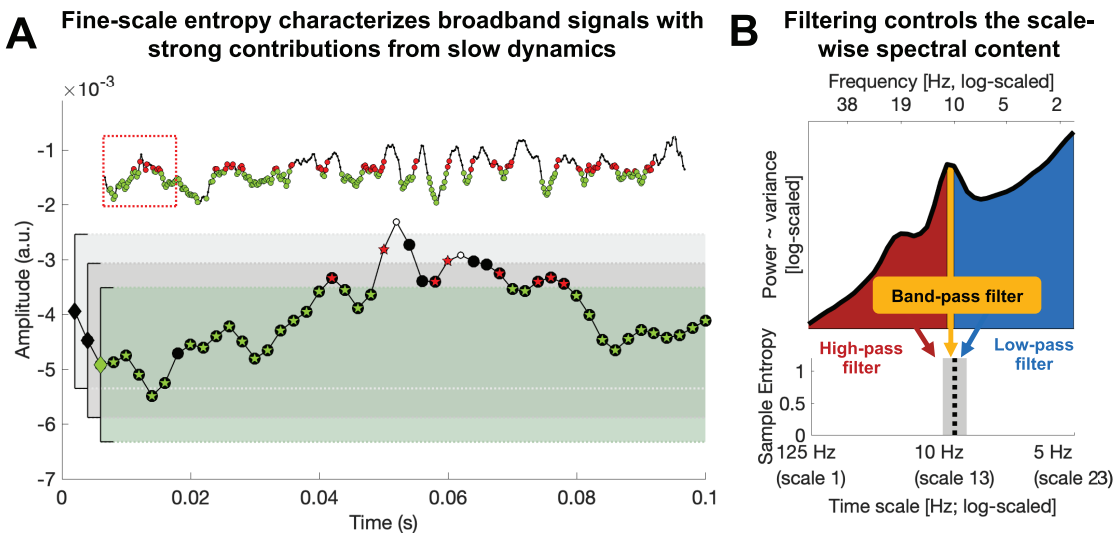

Fig 3. Issue 2: Traditional scale derivation leads to diffuse time-scale reflections of spectral power. (A) Exemplary sample entropy estimation in the same empirical EEG signal shown in Fig 1B, but without application of a high-pass filter, thus including dominant slow dynamics. See Figure 1B for a legend of the Figure elements. In brief, green elements indicate pattern matches at m+1, whereas red elements indicate pattern mismatches at m+1. In the presence of large low-frequency fluctuations, sample entropy at fine scales (here scale 1) may to a large extent characterize the temporal regularity of slow dynamics. Note that this is not a case of biased similarity bounds, but a desired adjustment to the large amplitude of slow fluctuations. The inset shows an extended segment (800 ms) of the same signal, allowing for an assessment of the slower signal dynamics. The red box indicates the 100 ms signal shown in the main plot. (B) A scale-wise filter implementation controls the scale-wise spectral content, as schematically shown here for the filter-dependent representation of spectral content at a time scale of approximately 10 Hz (for a note on the x-axis labeling, see methods: *Calculation of multi-scale sample entropy*). Traditionally, low-pass filters are used to derive coarser scales, which introduces a sensitivity to slower fluctuations. However, other filter implementations can be used to e.g., investigate the pattern irregularity of fast signal variations. No matter whether low or high pass filters are used, the spectral content influencing entropy

estimates is by definition not specific to any particular time scale; band-pass filters provide one viable solution permitting such specificity.

Narrowband rhythmic structure projected into simulated noise signals [1, 30, 35] provides a well-controlled situation in which to study the mapping of neural irregularity to MSE time scales, due to their clearly defined time scale (i.e., period = inverse of frequency) and regularity (added rhythmic variance = more regular signal = decreased entropy). Moreover, rhythmic structure remains a dominant target signal in neuroscience for which entropy, as a complementary descriptor, should provide an anti-correlated reflection. However, previous simulations on the mapping of rhythms onto MSE time scales have produced puzzling results that have received little attention in the literature so far; while a linear mapping between rhythmic frequency and entropy time scales has been observed, added rhythmic regularity has been shown to *increase* entropy above baseline in previous work [4, 18, 36]. This notably contrasts with the intuition that added signal regularity should reduce observed entropy. Thus, additional simulations are necessary to assess the intuitive notion that rhythmicity should be anticorrelated with entropy, and to investigate whether this phenomenon indeed occurs at specific time scales, as previously assumed [4, 18, 36]. In particular, we probed the feasibility of using high-pass and band-pass filters (relative to standard low-pass options) to control the MSE time scales at which rhythmicity would be reflected (Fig 3B).

In summary, Issue 1 suggests a coarse-scale bias introduced by global similarity bounds, and Issue 2 highlights broadband contributions to fine scales. In worst-case scenarios, a conjunction of these issues may lead to a reflection of fast dynamics in coarse entropy and a reflection of slow dynamics in fine entropy, thus paradoxically *inverting* the intuitive time scale interpretation. These issues have not been jointly assessed, however, and there is little evidence on the significance of these methodological issues for practical inferences.

Impact of issues on practical inferences: age differences in neural irregularity at fast and slow time scales

One principal application of multiscale entropy is in the domain of lifespan covariations between neural dynamics and structural brain network ontogeny [for a review see 37]. Within this line of inquiry, it has been proposed that structural brain alterations across the lifespan manifest as entropy differences at distinct time scales [12, 14, 32, 38]. Specifically, it has been suggested that coarse-scale entropy decreases and fine-scale entropy rises with increasing adult age as a reflection of senescent shifts from global to increasingly local information processing [12, 14]. Crucially, this mirrors observations based on spectral power, where age-related decreases in the magnitude of low-frequencies [39, 40] are accompanied by increases in high-frequency activity, conceptualized also as a flattening of power spectral density (PSD) slopes [12, 14, 32, 41]. These results seemingly converge towards a joint decrease of low-frequency power and coarse-scale entropy in older adults (and an increase for both regarding fast dynamics). However, this correspondence is surprising upon closer inspection given the presumed anticorrelation between the magnitude of signal regularity (as indicated by spectral power) and entropy. Given concerns regarding the interpretation of entropy time scales, we assessed cross-sectional age effects on both MSE and spectral power as a test case for potential mismatches in scale-dependent inferences.

Current study

Here, we aimed to address two issues of frequency-to-scale mapping and their relevance for empirical applications. First, we simulated variations in rhythmic power and frequency to probe the relationship between rhythmicity and MSE time scales. Primarily, our goal was to assess how global similarity bounds (Issue 1) and the scale-wise spectral content of the analyzed signal (Issue 2) influence the time scales at which added rhythmicity is observed. Then, we attempted to replicate reported cross-sectional age differences in human electroencephalography (EEG) signals recorded during rest. We assessed whether younger adults would show increased coarse scale and decreased fine-scale entropy compared to older adults, and we probed the extent to which such scale-specific results depend on mismatched spectral power via the issues above. Finally, we probed the possibility of deriving 'frequency-specific' estimates of signal irregularity, and assessed age differences therein. We refer to traditional settings that use global bounds and low-pass filtering as 'Original' throughout the remainder of the manuscript (see methods for details).

Results

Simulations indicate a diffuse mapping between rhythmicity and MSE time scales as a function of global similarity bounds and spectral signal content

Our first aim was to probe how scale-specific events, namely rhythms of a given frequency, modulate MSE time scales. For this purpose, we simulated 10 Hz (alpha) rhythms of varying power on top of pink noise and calculated the MSE of those signals. First, we probed the influence of global similarity bounds (as used in 'Original' implementations) on the time scale mapping (Issue 1). Crucially, as a result of using a global similarity bound for all time scales, strong rhythmic power decreased MSE estimates across a range of time scales, including time scales at which added 10 Hz rhythmicity did not contribute to the scale-wise signal (Fig 4A, upper panel). As highlighted in Issue 1, this can be explained by a general increase in the liberality of bounds (Fig 4A, lower panel) that introduced a bias on coarse-scale entropy below 10 Hz. In contrast, when scale-dependent similarity bounds were used with low-pass filters (Fig 4BC), strong rhythmicity systematically affected entropy only at finer time scales than the simulated frequency (i.e., to the left of the vertical line in Fig 4C, albeit in a diffuse manner, which we will examine next).

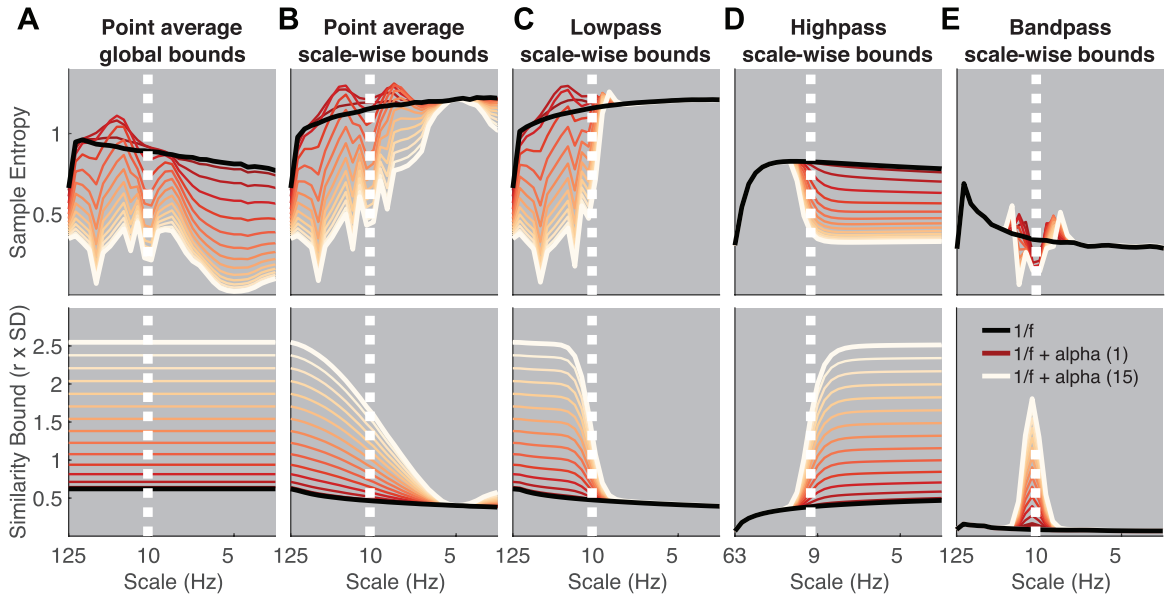

Fig 4. Rhythmic power manifests at different time scales depending on filter choice and similarity bound. Simulations indicate at which time scales the addition of varying magnitudes of stereotypic narrowband 10 Hz rhythms (blue-to-red line gradient) modulate entropy compared to the baseline 1/f signal (black line). Simulations indicate that increases in rhythmicity strongly reduce entropy estimates alongside increases in the similarity bound. The affected scales vary as a function of global vs. scale-dependent similarity bounds and the spectral filtering used to derive coarser time scales. Crucially, in 'Original' implementations, added narrowband rhythmicity decreased entropy with low scale-specificity, in line with global increases in the similarity bound (A). In contrast, the use of scale-varying thresholds (B) and dedicated filtering (C-E) increased specificity regarding the time scales at which rhythmicity was reflected. Note that timescales are presented in Hz to facilitate the visual assessment of rhythmic modulation. For all versions except high pass, the scale represents the upper Nyquist bound of the embedding dimension. For the high pass variant, the scale represents the high pass frequency (see methods). Time scales are log-scaled. Spectral attenuation properties of the Butterworth filters are shown in S4 Figure.

Second, we assessed the influence of the scale-wise filters (and hence, the spectral signal content) on frequency-to-scale mapping (see Issue 2, Fig 3B). In particular, we expected that low-pass filters (A-C) would lead to entropy decreases at finer time scales than the simulated frequency, whereas high-pass filters would lead to a rhythm representation at coarser time scales (Fig 3B). In line with these expectations, low-pass filters constrained the influence of narrowband rhythms to finer time scales (Fig 4C). As in previous work [29], Butterworth filters (Fig 4C) improved the removal of 10 Hz rhythms at coarser time scales and produced less aliasing compared with 'Original' point-averaging (see methods, Fig 4AB), with otherwise comparable results. Hence, low-pass filters rendered multiscale entropy sensitive to variance from low frequencies, suggesting that slow events (e.g. event-related potentials) are reflected in a diffuse manner across time scales. In contrast, high-pass filters constrained rhythm-induced entropy decreases to coarser time scales that included 10 Hz signal content, hence leading to estimates of high frequency entropy that were independent of low frequency power (Fig 4D). Finally, when band-pass filters were used (Fig 4E), rhythmicity decreased sample entropy at the target scales (despite producing edge artifacts surrounding the time scale of rhythmicity). In sum, these analyses highlight that rhythmic power increases will diffusely and non-specifically modulate MSE time scales as a function of the coarse-graining filter choice, unless a narrowband filter is applied.

Such diffuse reflection of rhythms across MSE time scales is at odds with previous simulations suggesting a rather constrained, linear mapping between the frequency of simulated rhythms and entropy time scales [4, 18, 36]. Furthermore, those studies indicated entropy *increases* with added rhythmicity, in contrast with the marked (and expected) decreases in entropy observed here. Crucially, increased entropy relative to baseline runs counter to the idea that the addition of a stereotypic pattern should decrease rather than increase pattern irregularity. To assess whether these seemingly divergent results can be reconciled, we repeated our simulation for different frequencies. We focused on a comparatively low level of rhythmicity (amplitude level = 2; SNR ~ 1.3 (see methods); S3 Figure displays exemplary time series), for which Fig 4A-C suggested transient entropy increases above baseline. Similar to previous reports, we observed a positive association between simulated frequencies and peak entropy time scales (Fig 5) across implementations, such that rhythms of a given frequency increased entropy at slightly finer time scales (see increases in entropy above baseline to the left of the dotted vertical lines in Fig 5A-C). However, as shown in Fig 4A-C, such increases were counteracted when rhythmic strength increased, while global *similarity bound*s (Fig 5A) liberally biased, and thus decreased, entropy at coarser time scales (i.e., to the right of the dotted lines in Fig 5A) independent of rhythmic strength. While the mechanistic origin of entropy increases remains unclear, previous conclusions may thus have overemphasized the scale-specificity of rhythmic influences.

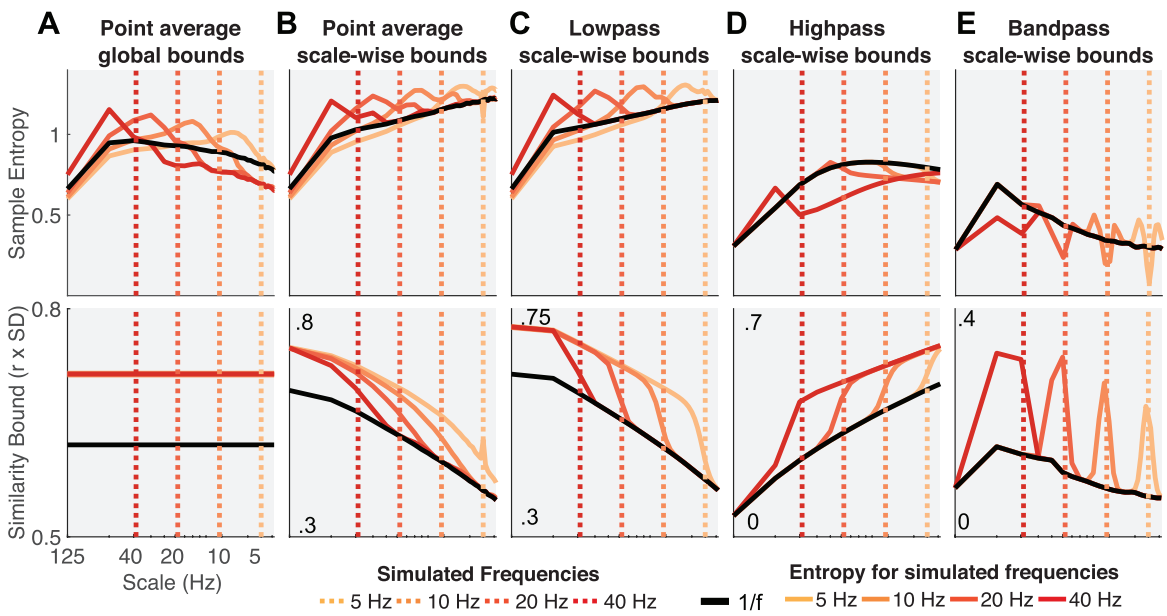

Fig 5. Influence of rhythmic frequency on MSE estimates and similarity bounds across different MSE variants. Simulations of different frequencies indicate a linear frequency-to-scale mapping of simulated sinusoids. Broken vertical lines indicate the simulated frequency. Low-pass MSE variants show increased entropy at time scales finer than the simulated frequency in combination with a global entropy decrease. Low-, high- and band-pass variants exhibit the properties observed in the alpha case, with a reduction above/below or at the simulated frequency. Time scales are log-scaled.

In sum, our simulations highlight that the choice of similarity bound and the signal's spectral content grossly affect one's ability to interpret MSE time scales. Our frequency-resolved

simulations suggest that a previously argued direct frequency-to-scale mapping is not tenable when typical estimation procedures are used.

Probing the impact of spectral power on MSE in a cross-sectional age comparison

Our simulations suggest profound influences of the choice of similarity bound (Issue 1) and spectral content (Issue 2) on scale-dependent MSE estimates. However, whether these issues affect inferences in empirical data remains unclear. Entropy differences across the lifespan are an important application [6], where 'Original' MSE implementations suggest that older adults exhibit higher entropy at finer time scales and lower entropy at coarser time scales compared to younger adults [for a review see 37]. Importantly, a shallowing of PSD slopes with age has also been reported, as represented by higher power at high frequencies and lower power at low frequencies [32, 41]. The raised issues of a potential (1) reflection of high frequency power on coarse scales and (2) diffuse reflection of slow spectral content thus question whether traditional MSE group differences reflect veridical differences in signal irregularity at matching time scales. Given those two issues, we specifically hypothesized that:

(A) Adult age differences in coarse-scale MSE can be accounted for by group differences in high frequency power, due to the typical use of global similarity bounds (Issue 1).
(B) Adult age differences in fine-scale MSE reflect differences in PSD slopes and thus depend on the contribution of low frequencies to broadband signals (Issue 2).

To assess these hypotheses, we first attempted to replicate previously reported scale-wise age differences in MSE and spectral power during eyes open rest. 'Original' settings replicated scale-dependent entropy age differences (Fig 6A1). Specifically, compared with younger adults, older adults exhibited lower entropy at coarse scales, and higher entropy at fine scales (Fig 6A1). Mirroring these results in spectral power, older adults had lower parieto-occipital alpha power and increased frontal high frequency power (Fig 6A2) compared to younger adults. This was globally associated with a shift from steeper to shallower PSD slopes with increasing age (Fig 6D). At face value, this suggests joint shifts of both power and entropy, in the same direction and at matching time scales. Crucially, however, the spatial topography of entropy differences inverted the time scale of power differences (Fig 6B & C; cf., upper and lower topographies), such that frontal high frequency power topographies resembled coarse entropy topographies (Fig 6B), while parieto-occipital age differences in slow frequency power resembled fine-scale entropy differences (Fig 6D). This rather suggests scale-mismatched associations between entropy and power.

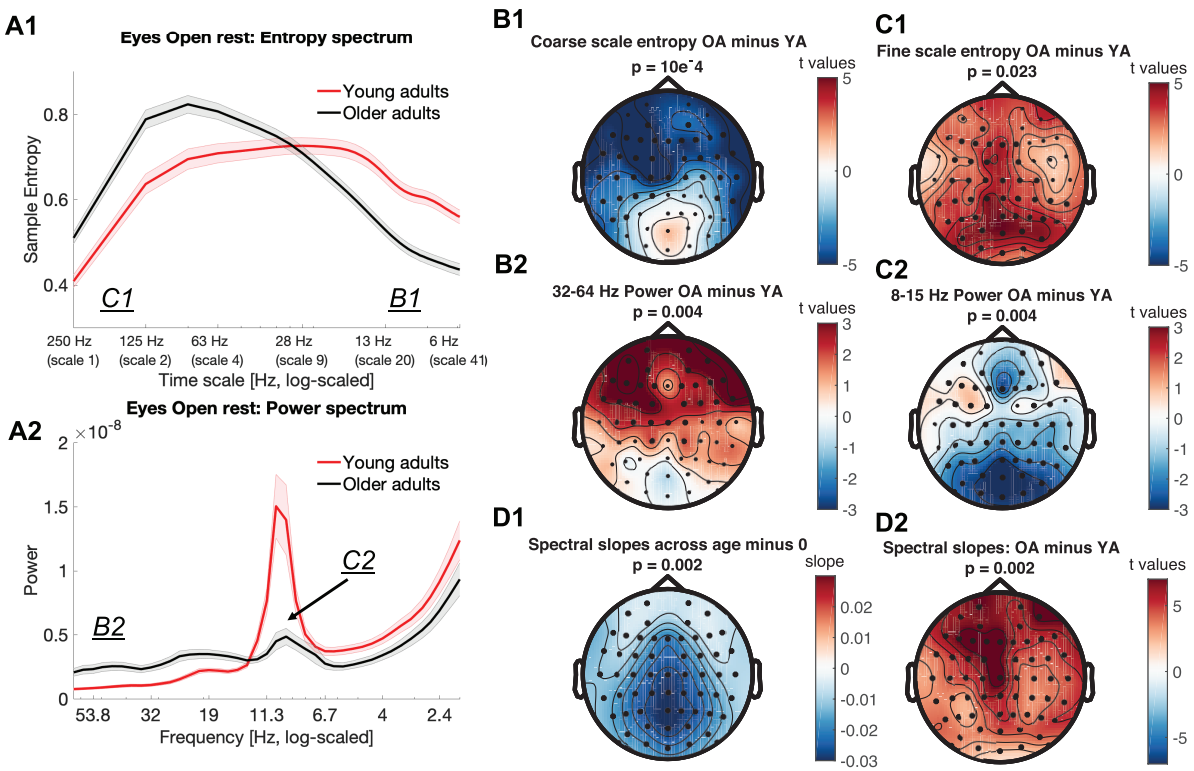

Fig 6. Timescale-dependent age differences in spectral power and entropy during eyes open rest. (A) MSE (A1) and power (A2) spectra for the two age groups. Error bars show standard errors of the mean. Note that in contrast to standard presentations of power, the log-scaled x-axis in A2 is sorted by decreasing frequency to enable a better visual comparison with entropy time scales (see also Fig 2D). T-values of power age contrast are shown in S5 Figure. (B, C) Topographies of age differences indicate mirrored age differences in fast entropy and low frequency power, as well as coarse entropy and high frequency power. Significant differences are indicated by asterisks. (D1) Spectral slopes across age groups. (D2) Age differences in spectral slopes.

Next, we assessed the impact of scale-wise similarity bounds and different scale-wise filters on the indication of MSE age differences (Fig 7).

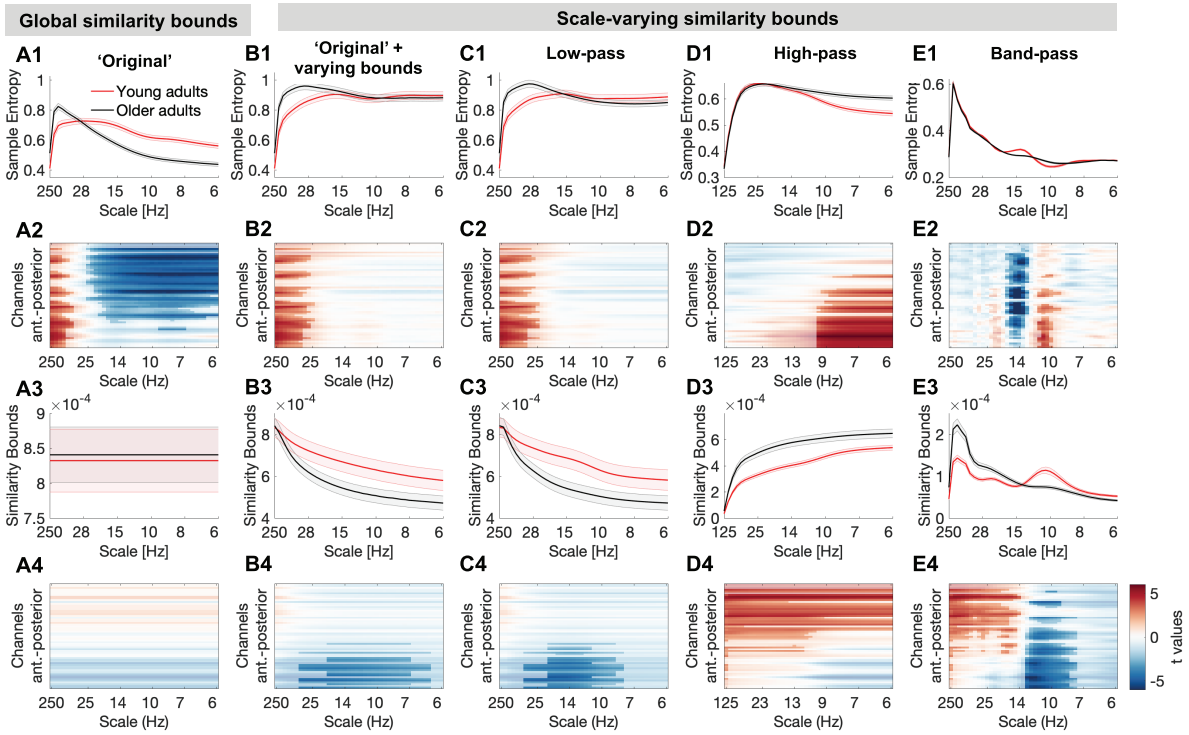

Fig 7. Multiscale entropy age differences depend on the specifics of the estimation method. Grand average traces of entropy (1st row) and similarity bounds (3rd row) alongside t-maps from statistical contrasts of age differences (2nd + 4th row). Age differences were assessed by means of cluster-based permutation tests and are indicated via opacity. Original MSE (A) replicated reported scale-dependent age differences, with older adults exhibiting higher entropy at fine scales and lower entropy at coarse scales, compared with younger adults. The coarse-scale difference was exclusively observed when using global similarity bounds, whereas the fine-scale age difference was indicated with all low-pass versions (A, B, C), but not when signals were constrained to high-frequency or narrow-band ranges (D, E). In contrast, narrowband MSE indicated inverted age differences within the alpha and beta band (E).

Briefly, we observed three main results that deserve highlighting:

(A) The implementation of scale-wise similarity bounds affected MSE age differences (Fig 7; Hypothesis A; Issue 1). In particular, with global bounds, MSE indicated increased fine-scale and decreased coarse-scale entropy for older compared to younger adults (Fig 7A1 and A2), in the absence of group differences in the global *similarity bound* (Fig 7A3 and A4). In contrast, scale-varying bounds captured age differences in variance at finer scales (Fig 7B) and abolished age differences in coarse-scale entropy (effect size was significantly reduced from r = .58 to r = .07; p=6.8*10^-5; see Statistical analyses).

(B) The chosen scale-wise filtering method also affected MSE age differences (Hypothesis B; Issue 2). Specifically, fine-scale entropy age differences were indicated when low-pass filters rendered those scales sensitive to low-frequency content (Fig 7B/C). Effect size did not significantly change with the adoption of scale-varying similarity bounds (from r = .44 to r = .45; p=.934). In contrast, when high-pass filters constrained fine scales to high frequency signals (Fig 7D), no fine-scale age differences were observed and the age effect was significantly reduced to r = .09 (p = .008).

(C) Strikingly, the implementation of narrowband filters (Fig 7E) indicated two unique age effects not recoverable using other approaches: larger 'narrowband' alpha-band entropy and lower beta-band entropy for older adults compared with younger adults.

In the following sections, we assess these results more closely.

Global similarity bounds bias coarse-scale entropy to reflect high-frequency power

Scale-dependent entropy effects in the face of global similarity bounds (as observed in the 'Original' implementation; Fig 7A) may intuitively suggest scale-specific variations in signal irregularity in the absence of variance differences. However, global similarity bounds increasingly diverge from the scale-wise signal variance towards coarser scales (Issue 1; Fig 8A). This introduces a liberal bias that systematically varies as a function of the removed variance, thereby rendering coarse MSE scales sensitive to differences in higher frequency power (i.e., Issue 1), as observed in the case of aging (Fig 8A & B).

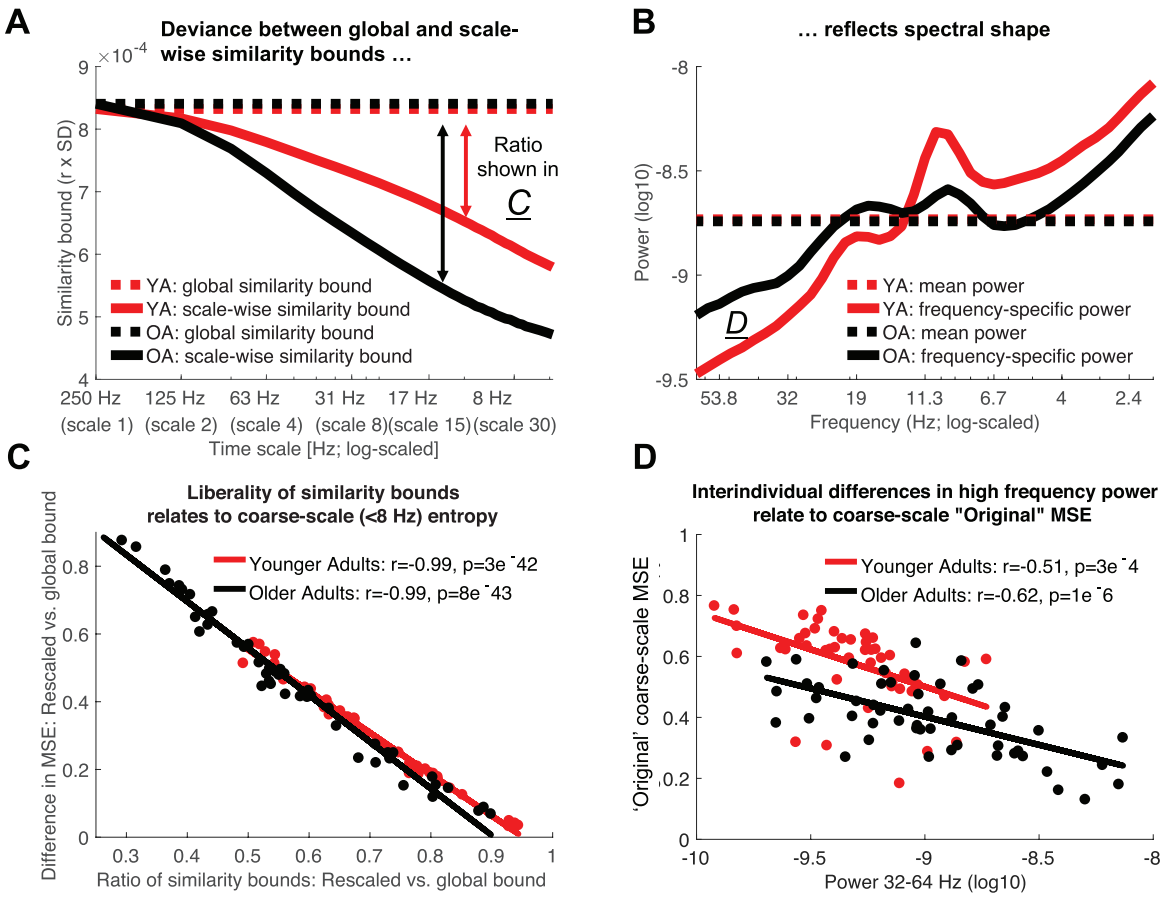

Fig 8. Divergence of scale-specific signal variance from global similarity bounds accounts for age differences in coarse-scale entropy. (A, B) A global similarity bound does not reflect the spectral shape, thus leading to disproportionally liberal criteria at coarse scales following the successive removal of high-frequency variance (see Fig 2D-F for the schematic example). Scale-dependent variance is more quickly reduced in older compared to younger adults (A) due to the removal of more prevalent high-frequency variance in the older group (B). This leads to a differential bias across age groups, as reflected in the differentially mismatched distance between global and scale-dependent similarity bounds at coarser scales. (C) Removing this bias by adjusting the similarity bounds to the scale-dependent signal is associated with increases in coarse-scale entropy. This shift is more pronounced

in older adults following the removal of a more prevalent bias. (D) With global similarity bounds, coarse-scale entropy strongly reflects high frequency power due to the proportionally more liberal similarity threshold associated. Low frequency power < 8 Hz was not consistently related to coarse-scale entropy (log10-power as in D; *YA: r = .12; p = .419; OA: r = .36, p = .009*). Data in A and B are global averages, data in C and D are averages from frontal Original effect cluster (see Fig 4B) at entropy time scales below 6 Hz.

To assess whether global bounds introduced an association between high frequency power and coarse scale entropy in the case of aging, we probed changes in *similarity bounds* and MSE between the use of global and scale-varying bounds. As expected, we observed a strong anti-correlation between inter-individual changes in *similarity bounds* and MSE (Fig 8C). That is, the more similarity bounds were re-adjusted to match the scale-wise variance, the more entropy estimates increased. Crucially, this difference was more pronounced for older adults (paired t-test; r: p = 5e-6; MSE: p = 3e-4). Due to their increased high frequency power, coarse-graining decreased older adults' scale-wise variance more so than younger adults' variance. Thus, global similarity bounds presented a more liberal threshold at coarser scales for older adults than for younger adults, in turn producing lower MSE estimates. In line with this assumed link between high frequency power and coarse scale entropy as a function of global bounds, individual high frequency power at frontal channels was anticorrelated with coarse-scale entropy estimates when a global similarity bound was applied (Fig 8D), but was dramatically weaker when the similarity bound was recomputed for each scale (YA: r = -0.15; p = .302; OA: r = .20, p = .146). This is in line with our observation that coarse-scale age differences (Fig 7A) were not found when scale-wise bounds were used (Fig 7B).

Taken together, these results indicate that increased high frequency power with age can account for entropy decreases at coarse time scales, whereas the pattern irregularity of slow dynamics *per se* was not modulated by age.

Low-frequency contributions render fine-scale entropy a proxy measure of PSD slope

A common observation in the MSE literature is that MSE is highly sensitive to task and behavioral differences at fine time scales, which are assumed to reflect fast dynamics. This is surprising given that high-frequency activity remains challenging to measure [42]. Moreover, previous studies suggest that fine-scale entropy reflects power spectral density (PSD) slopes [e.g., 10, 32]. Given that 'Original' MSE implementations contain both high- and low-frequency components due to the assessment of broadband signals, we probed whether fine-scale associations with PSD slopes depend on the presence of slow fluctuations and whether age-related slope variations can account for fine-scale entropy age differences (Hypothesis B).

As expected, individual fine-scale entropy was strongly and positively related to PSD slopes (Fig 9A) in both younger and older adults. Notably, after high-pass filtering the signal, the positive relation of fine-scale entropy to PSD slopes disappeared in both age groups (Fig 9B, dotted lines), and turned negative in older adults (see S6 Figure), while age differences in fine-scale entropy disappeared (Fig 7D). Relations between entropy and PSD slopes – and age differences – re-emerged once low-frequency content was included in the entropy estimation (Fig 9C, dashed lines), indicating that the presence of slow fluctuations was necessary for PSD slope relations. To assess whether varying PSD slopes accounted for fine-scale age differences in 'Original' MSE, we computed partial correlations between the measures. No significant

prediction of age group status by fine-scale entropy was observed when controlling for the high collinearity with PSD slopes (r = -.06, p = .59), whereas PSD slopes significantly predicted age group status when controlling for MSE (r = .38, p <.001).

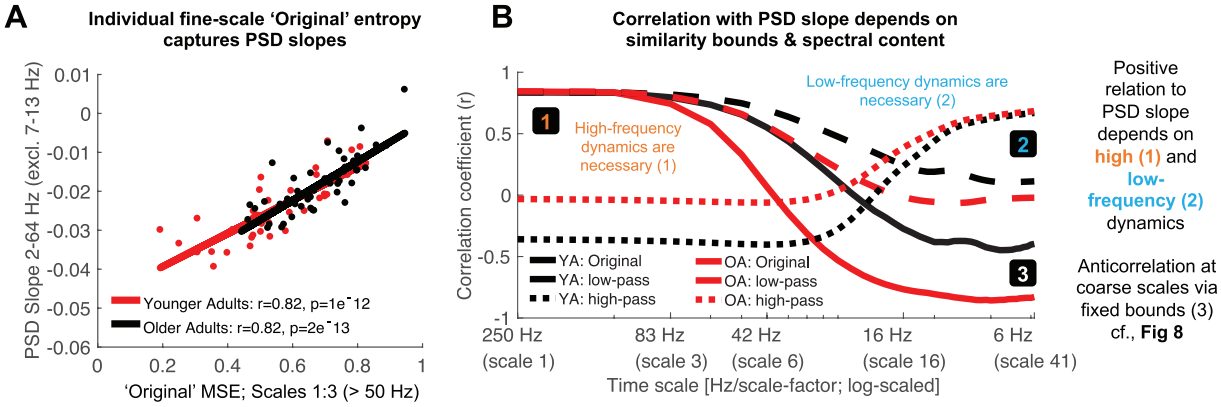

Fig 9. The presence of low- and high-frequency content renders fine entropy slopes sensitive to PSD slopes. A) Sample entropy at fine time scales represents the slope of power spectral density across age groups. The 7-13 Hz range was excluded prior to the PSD slope fit to exclude the rhythmic alpha peak (see Fig 8B). (B) The presence of both slow and fast dynamics is required for positive associations with PSD slopes to emerge. The direction and magnitude of correlations of scale-wise entropy with PSD slopes depends on the choice of global vs. rescaled similarity bounds, as well as the choice of filtering. Original entropy inverts from a positive correlation with PSD slope at fine scales to a negative association at coarse scales. Rescaling of the similarity bound abolishes the negative correlation of coarse-scale entropy with PSD slopes. S6 Figure presents scatter plots of these relationships. The x-axis indicates the upper frequency bounds for the low-pass version.

Finally, spectral slopes were anticorrelated with coarse-scale entropy when global similarity bounds were used (Fig 9C, solid lines), but not when criteria were scale-wise re-estimated (Fig 9C, dashed and dotted lines). This again suggests a presence of the scale-wise bias noted in Issue 1 (i.e., scale-wise bound divergence); subjects with shallower slopes (more high frequency power) had increasingly liberally-biased thresholds at coarser scales, resulting in overly low entropy estimates.

In sum, age differences in fine-scale entropy were conditional on the presence of both low- and high-frequency dynamics and reflected differences in PSD slopes; while the pattern irregularity of fast dynamics *per se* was not modulated by age.

Narrowband MSE indicates age differences in signal irregularity in alpha and beta band

The previous analyses highlighted how the spectral content of the signal can give rise to MSE time scale mismatches. However, our simulations also suggest a far more accurate mapping between entropy and power when scale-wise bandpass filters are used (Fig 4A). Concurrently, application of the band-pass implementation indicates a partial decoupling between entropy and variance (as reflected in the *similarity bound*) age differences (Fig 7E). Specifically, older adults exhibited higher parieto-occipital entropy at alpha time scales (~8-12 Hz) and lower central entropy at beta time scales (~12-20 Hz) than in younger adults (Fig 7; Fig 10AB). Whereas alpha-band entropy was moderately and inversely correlated with alpha power (Fig 10C) and the age difference was inversely reflected in the similarity bound in a topographically similar fashion (Fig 10E), the same was not observed for entropy in the beta range for both age groups (Fig 10DF). Promisingly, this indicates evidence for what many who

employ MSE measures in cognitive neuroscience presume – that power and entropy *can* be decoupled, providing complementary signatures of neural dynamics.

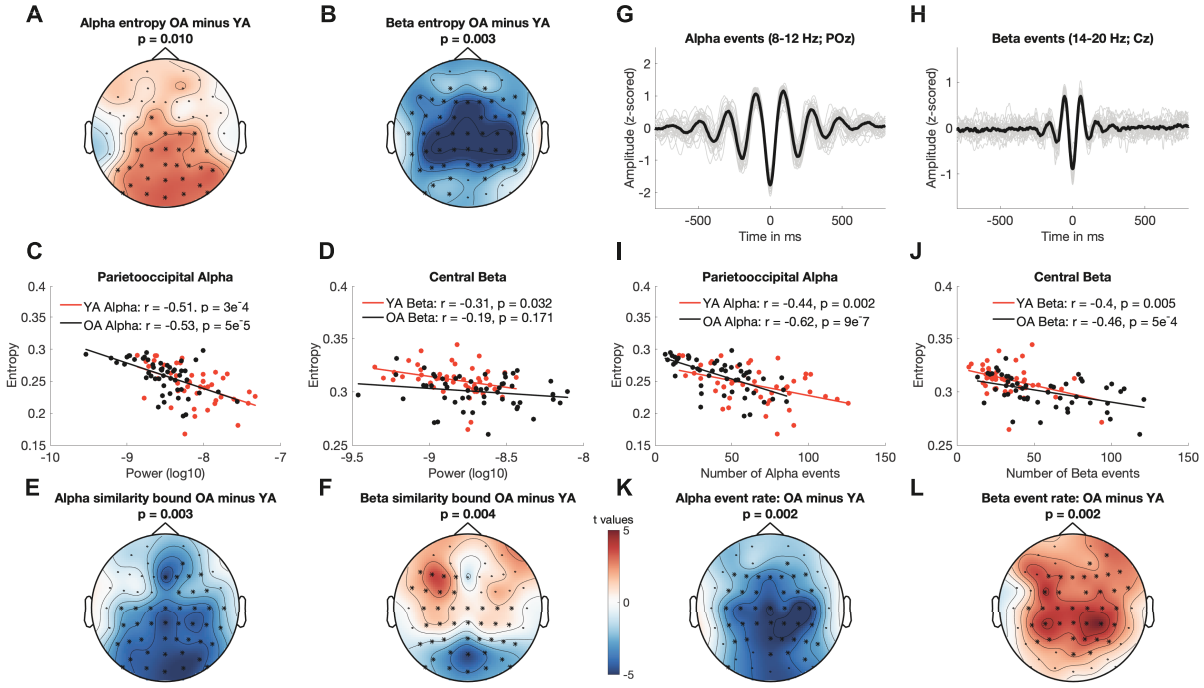

Fig 10. Narrowband MSE reflects age differences in alpha- and beta-specific event (ir)regularity. (A, B) Narrowband MSE indicates age differences in the pattern complexity at alpha (A) and beta (B) frequencies. (C, D) Alpha, but not beta power consistently correlates negatively with individual narrowband entropy within clusters of age differences. (E, F) Similarly, alpha but not beta similarity bounds show an inverted age effect with similar topography. (G, H) Single-trial rhythm detection highlights a more transient appearance of beta compared with alpha events. (I, J) The rate of stereotypical single-trial alpha and beta events is anticorrelated with individual narrowband entropy. (K, L) The rate of spectral events exhibits age differences that mirror those observed for entropy.

This divergence of entropy and power in the beta band is particularly interesting as beta events have been observed to exhibit a more transient waveform shape [43, 44], while occupying a lower total duration during rest than alpha rhythms [34]. Indeed, it should be the rate of stereotypic spectral events that reduces pattern irregularity rather than the overall power within a frequency band. To better test this assumption in our data, we applied single-trial rhythm detection to extract the individual rate of alpha (8-12 Hz) and beta (14-20 Hz) events. As predicted, alpha events had a more sustained appearance compared with beta events as shown in Fig 10G & H (events were time-locked to the trough of individual events; see methods). Importantly, both alpha and beta event rate were inversely and moderately correlated with entropy estimates (Fig 10IJ) at matching time scales in the band-pass version. Correlations were also numerically higher than between power and entropy (Fig 10C and D), suggesting that entropy captured the non-stationary character of the rhythmic episodes that are not captured by sustained power estimates. The relationships remained stable after controlling for individual event rate and entropy in the age effect cluster of the other frequency band (partial correlations: alpha for younger adults: r = -.52, p = 2e-4; alpha for older adults: r = -.71, p = 8e-9; beta for younger adults r = -.49, p = 6e-4; beta for older adults: r = -.56, p = 2e-5), indicating separable associations between event rate and entropy between the two frequency bands. This is important, as our simulations suggest increased entropy estimates around narrow-band filtered

rhythmicity (see Fig 4A). Furthermore, a permutation test indicated age differences in beta rate that were opposite in sign to the entropy age difference (see Fig 10L). In particular, older adults had a higher number of central beta events during the resting state compared with younger adults, thus rendering their beta-band dynamics more stereotypic. In sum, these results suggest that narrowband MSE estimates approximate the irregularity of non-stationary spectral events at matching time scales.

Discussion

MSE aims to characterize the temporal irregularity of (neural) time series at multiple temporal scales. In the present study, we have highlighted two primary issues that may render the interpretation of time scales unintuitive in traditional applications: (Issue 1) biases from global similarity bounds, and; (Issue 2) the characterization of broadband, low-frequency dominated signals (see Fig 11A for a schematic summary). In the following, we discuss these effects and how they can impact traditional inferences regarding signal irregularity, in particular with regard to empirical age differences. Then, we discuss age effects in narrowband signal irregularity at interpretable temporal scales. Finally, we recommend procedures to improve scale-specific MSE inferences.

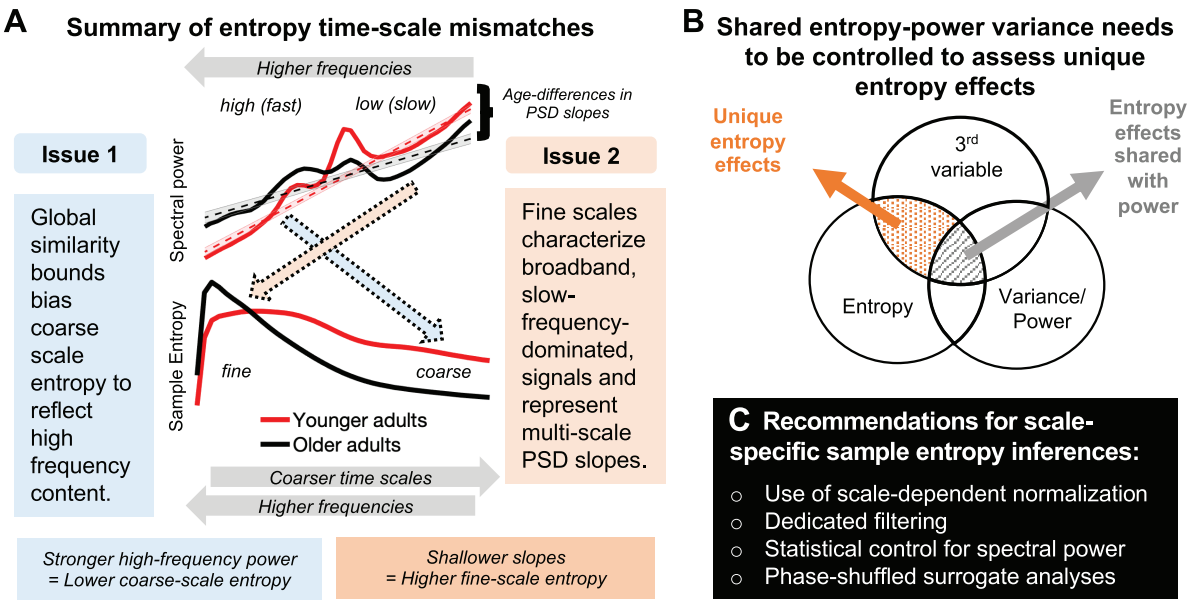

Fig 11. Summary of the identified time-scale mismatches and recommendations for future studies. (**A**) We highlight two scale-dependent mismatches that run counter to the intuition that entropy at fine scales primarily refers to fast dynamics, and vice-versa: (1) Coarse-scale entropy is biased towards reflecting high-frequency content when signals of decreasing variance are compared to a global, and increasingly inadequate, similarity bound. (2) Fine-scale entropy characterizes scale-free 1/f slopes when broadband signals include slow frequency content. (**B**) Beyond time-scale mismatches, entropy and variance can often be collinear, in part due to their shared description of linear signal characteristics, such as rhythmicity. To identify complementary and unique relations of pattern complexity compared to more established measures of variance, explicit statistical control is required for the latter. (**C**) We propose multiple strategies to safeguard future applications against the highlighted issues.

571 **Issue 1: Global similarity bounds bias coarse-scale entropy estimates**

572 Coarse scale entropy is commonly thought to represent the irregularity of slow dynamics.
573 However, MSE's traditionally global similarity bounds systematically bias coarse scale entropy
574 estimates. Given that scale-wise variance decreases across scales, the liberality of global
575 similarity bounds increases, causing entropy to decrease despite no ostensible shift in pattern
576 irregularity. This bias is independent of the values of the global similarity bound – which did
577 not differ across groups here – but rather depends on the *removed* variance at the time scale of
578 interest. This issue has led to puzzling results in past work. For example, several papers using
579 typical forms of ('original') MSE have shown that in white noise signals (which by definition
580 should be equally irregular at all time scales), entropy appears to unintuitively decrease towards
581 coarser scales, whereas pink noise signals undergo less entropy reduction across initial scales
582 due to the removal of less high-frequency content [25]. Strikingly, such puzzling effects have
583 been used to *validate* the most common implementation of MSE [e.g., 23, 28] rather than to
584 indicate the presence of a systematic bias in estimation. This appears motivated by the
585 assumption that "changes of the variance due to the coarse-graining procedure are related to the
586 temporal structure of the original time series, and should be accounted for by the entropy
587 measure" [8]. We rather consider the similarity bound divergence as a clear bias for the intuitive
588 interpretation of time scales in MSE applications.
589 Importantly, this bias affects practical inferences. In the current resting-state EEG data, an
590 age-related increase in high frequency power manifested unintuitively as a decrease in coarse-
591 scale entropy via systematic group differences in the divergence of similarity bounds. Note that
592 we presume that this age difference arises from a relative bias. As such, variations in high-
593 frequency power suffice, even at low levels in 1/f scenarios, to systematically impact coarse-
594 scale estimates and to specifically explain variance in a third variable of interest (e.g., age; see
595 Fig 11B). Given that global similarity bounds remain prevalent in applications (see S1 File),
596 we hope that our practical example motivates the adoption of scale-varying parameters. Overall,
597 we perceive little justification for the use of scale-invariant parameters in MSE estimation in
598 future work.

599 **Issue 2: Fine-scale entropy relates to PSD slopes in the presence of slow frequency**
600 **content**

601 While fine-scale entropy is often interpreted as a signature of "fast" temporal irregularity,
602 it is typically estimated from broadband signals. As such, fine (or single) scale entropy has been
603 proposed as a signature of desynchronized cortical states [32, 45] that feature a suppression of
604 low-frequency power with concurrent increases in the magnitude of high frequency dynamics
605 [46-48]. This synergy is thought to benefit local information processing by regulating cortical
606 gain as a function of the local excitation-inhibition (E/I) balance. Spectral (PSD) slopes,
607 characterizing the scale-free 'background' or 'noise' component of the total variance, and have
608 been proposed as an index of such E/I balance [41, 49, 50]. By linking fine-scale entropy to
609 PSD slopes, we replicated previous observations of increasing fine-scale entropy with
610 shallower slopes [10, 13, 25, 32, 51] and shorter temporal autocorrelations [4, 23, 52]. However,

we qualify this association by highlighting that the *joint* presence of slow and fast dynamics in the signal is necessary to produce such effects.

The association between broadband signal entropy and spectral slopes coheres with the notion that shallower slopes have a more 'noisy' or irregular appearance in the time domain. Thus, spectral slopes and temporal irregularity may be conceptualized – at least in part – as different perspectives on the same signal characteristics. Practically however, the correspondence between fine-scale entropy and 1/f slopes should nonetheless be tested, given that these scales are also sensitive to other signals characteristics, such as narrowband rhythmicity (as shown in our simulations). In sum, our analyses provide insights into the sensitivity of fine-scale entropy to desynchronized cortical states and highlight the surprising importance of slow fluctuations for such associations.

Spectral power and entropy: What's irregularity got to do with it?

For entropy to be a practical and non-redundant measure in cognitive neuroscience, both its convergent and discriminant validity to known signal characteristics should be established. Multiple features can influence the temporal irregularity of neural time series. These include traditional 'linear' PSD features, (e.g., temporal autocorrelation, rhythmicity, etc.) as well as 'non-linear' features (e.g., phase resets, cross-frequency coupling, etc.). It is therefore worth noting that associations between spectral power characteristics and entropy estimates are partly anticipated (Fig 11B). For example, as noted before, entropy should reduce with increased rhythmic irregularity, and increase with shallowing of PSD slopes (and hence, shortening of temporal autocorrelations). However, the use of MSE is often motivated by its perceived sensitivity to non-linear properties of brain dynamics that cannot be captured by traditional PSD analyses [e.g., 53, 54, 55]. In extreme cases, an independence between estimates may sometimes be erroneously inferred from the use of variance-based similarity bounds. Contrary to such orthogonality assumptions, our analyses highlight that differences in spectral variance (as captured by the similarity bound, which is typically neglected as a measure of interest when estimating MSE) may account for a large proportion of reported MSE effects [see also appendix in 23]. As such, non-linear characteristics *per se* may often do little to drive MSE estimates.

Relevance of identified time scale mismatches to previous work

Although the highlighted issues broadly apply to applications in which MSE is a measure of interest (e.g., assessment of clinical outcomes [e.g., 18]; prediction of cognitive performance [e.g., 38]), our results are also especially relevant for MSE differences across the lifespan. Previous applications indicated that older adults exhibit lower coarse-scale entropy and higher fine-scale entropy compared with younger adults [12, 14, 23]. In the power spectrum, these effects were inverted, with older subjects showing enhanced high-, and reduced low-frequency power. This was previously taken as evidence that older adults' high-frequency dynamics were not only enhanced in magnitude, but also more unpredictable compared with younger adults' dynamics. While we replicate similar results here when standard MSE implementation are applied, our analyses question the validity of previous interpretations. In particular, our results suggest that age-related increases in coarse-scale entropy do not reflect differences in the

irregularity of slow dynamics, but rather reflect differential high frequency power. An absence of age differences at coarse scales is in line with previous work with scale-wise similarity bounds [15]. Similarly, our analyses indicate that differences in fine-scale 'pattern irregularity' describe age-related changes in PSD slopes, which themselves reflect a shift from distributed to local processing. Taken together, our results suggest that entropy age differences dominantly arise from differences in the PSD spectrum, and appear at counterintuitive time scales. This is further in line with a previous application using surrogate data that highlighted that age group differences were mainly captured by linear auto-correlative properties [see appendix in 23].

Cross-sectional age differences in narrowband MSE

Complementing traditional broadband applications, our use of narrowband MSE suggested age-related entropy increases in the posterior-occipital alpha band and decreases in central beta entropy that inversely tracked the regularity of alpha and beta events, respectively. Posterior-occipital decreases in alpha power and frequency with age are fundamental findings in many age-comparative studies [56]. While age-related increases in beta power are not observed as consistently [see e.g., 56 for a review], age-related increases in their prevalence have been observed during eyes open rest [57]. In addition, beta power increases over contralateral motor cortex during rest may reflect greater GABAergic inhibition in healthy aging [58]. While our results are not hemisphere-specific, they may similarly reflect increased inhibition in older adults, potentially reflected in an increased number of stereotypical beta events [44]. As our aims were methods-focused in the present study, the functional interpretation of our observed age differences necessitates caution pending further research. Nevertheless, these results highlight that scale-specific narrowband filtering can provide novel, frequency-specific, insights into event/signal irregularity.

Recommendations for future applications

The issues raised here suggest that additional steps need to be taken to achieve valid scale-wise estimates of MSE, and to support the perceived complementary nature of MSE relative to more typical measures (such as spectral power, etc.):

a) We see little motivation for the use of global similarity bounds as they introduce challenges rather than benefits. We therefore recommend the field abandons global *similarity bound*s in MSE applications.
b) We recommend spectral filters to validate the scale-specificity of effects. For example, if effects are observed at fine temporal scales with a low-pass filter, additional high-pass filters may inform about the spectral extent of the effect. For entropy estimates of slow dynamics, traditional low-pass filter settings already apply this principle by becoming increasingly exclusive to slow fluctuations (if scale-dependent normalization is used). If the signal is filtered into dedicated frequency ranges, inferences regarding pattern irregularity become narrowband-specific. While this narrowband entropy by definition enforces a more rhythmic appearance than the raw signal may convey [59] and thus cannot capture multi-scale properties at any single scale, it may nevertheless provide a complementary index of frequency-specific variability.

c) We regard statistical control as necessary to establish entropy effects that are not capturable by traditional linear indices (such as PSD characteristics). While some studies have shown joint effects of interest in MSE and (band-limited) spectral power [11, 12, 14, 15, 60-66], others identified unique MSE effects [18, 67-69]. However, the (mis)match between time-scales and frequencies may not always be readily apparent, at least in part due to the various issues raised here. As shown here, controls should include both narrowband ('rhythmic') power and the arrhythmic signal background. As the scale-wise *similarity bound* is used for normalization, it should at the very least be controlled for. The choice of features may further be aided by comparing effect topographies of spectral power and entropy, as done in the present study. An important point to note is the relevance of statistical controls for relations to third variables (see Fig 11B). While some studies highlight scale-dependent associations of entropy with power, a large amount of shared variance (e.g., of coarse-scale entropy with slow frequency power) does not guarantee that a smaller portion of residual variance (e.g., shared with normalization biases) systematically does or does not relate to other effects of interest. This is equally relevant for identifying unique non-linear contributions. For example, while we observed moderate associations between band-specific rhythm events and entropy here, this non-redundant association nevertheless leaves room for the two measures to diverge in relation to third variables. This is in line with prior work [23, 70] showing that despite a dominant influence of linear characteristics on entropy estimates, non-linear contributions can uniquely explain a (smaller) portion of entropy variance.

d) Finally, a principled way to dissociate non-linear signal characteristics from linear signal variance is to use phase-shuffled surrogate data [5, 71-74]. Phase randomization effectively alters original time series patterns while preserving linear PSD characteristics and "is unavoidable if conclusions are to be drawn about the existence of nonlinear dynamics in the underlying system" [5]. While such surrogate approaches have been utilized in select entropy applications [4, e.g., appendix of 23] to highlight entropy's non-linear sensitivity [e.g., 26, 28], it has not become common practice in application. Given that spectral power can impact MSE in many ways, of which some are shown here, we consider surrogate analyses as an optimal approach to verify the contribution of non-linear signal characteristics.

In combination, such controls may go a long way toward establishing unique, complementary, and valid contributions of MSE in future work.

Conclusions

Many inferences regarding multiscale entropy in cognitive/clinical neuroscience rely on the assumption that estimates uniquely relate to pattern irregularity at specific temporal scales. Here we show that both assumptions may be invalid depending on the consideration of signal normalization and spectral content. Using simulations and empirical examples, we showed how spectral power differences can introduce entropy effects that are inversely mapped in time scale (i.e., differences in the high frequency power may be reflected in coarse entropy and vice versa; see Fig 11A). As these results suggest fundamental challenges to traditional MSE analysis

procedures and inferences, we highlight the need to test for unique entropy effects (Fig 11B) and recommend best practices and sanity checks (Fig 11C) to increase confidence in the complementary value of pattern irregularity for cognitive/clinical neuroscience. While the warranted claim has been made that "it would be unreasonable simply to reduce sample entropy to autocorrelation, spectral power, non-stationarity or any of their combinations" [4], this should not mean that we cannot test whether one or more of these contributors may sufficiently explain MSE effects of interest. We thus propose that MSE effects may be taken as a starting point to explore the linear and nonlinear features of brain signals [e.g., 76]. We believe that empirical identification of the unique predictive utility of MSE will advance the quest for reliable mechanistic indicators of flexible brain function across the lifespan, and in relation to cognition, health, and disease.

Methods

Simulations of relations between rhythmic frequency, amplitude, and MSE

To assess the influence of rhythmicity on entropy estimates, we simulated varying amplitudes (0 to 7 arbitrary units in steps of 0.5) of 10 Hz (alpha) rhythms on a fixed 1/f background. This range varies from the absence to the clear presence of rhythmicity (see S3 Figure for an example). The background consisted of $\frac{1}{f^x}$-filtered Gaussian white noise (mean = 0; std = 1) with x = 1 that was generated using the function f_alpha_gaussian [77]. The background was additionally band-pass filtered between .5 and 70 Hz using 4th order Butterworth filters. Eight second segments (250 Hz sampling rate) were simulated for 100 artificial, background-varying trials, and phase-locked 10 Hz sinusoids were superimposed. To analyze the reflection of rhythmic frequency on time scales and to replicate a previously observed linear frequency-to-timescale mapping between the spectral and entropy domains [4, 18, 36], we repeated our simulations with sinusoids of different frequencies (5 Hz, 10 Hz, 20 Hz, 40 Hz, 80 Hz), that covered the entire eight second-long segments. For a specified amplitude level, the magnitude of frequency-specific power increases (or narrowband signal-to-noise ratio) increased alongside simulated frequencies due to the decreasing frequency power of pink noise, while the ratio of rhythmic-to-global signal variance (or global signal-to-noise ratio (SNR)) remained constant across simulated frequencies. We used the following definition: $\mathrm{SNR}_{\mathrm{global}} = \left(\frac{RMS_{signal}}{RMS_{noise}}\right)^2$, where RMS_{noise} is the root mean square of the pink noise time series and RMS_{signal} characterizes the pink noise signal with added rhythmicity.

Resting state data and preprocessing

To investigate the influence of similarity bounds and filter ranges in empirical data, we used resting-state EEG data collected in the context of a larger assessment prior to task performance and immediately following electrode preparation. Following exclusion of three subjects due to recording errors, the final sample contained 47 younger (mean age = 25.8 years, SD = 4.6, range 18 to 35 years; 25 women) and 52 older adults (mean age = 68.7 years, SD = 4.2, range 59 to 78 years; 28 women) recruited from the participant database of the Max Planck Institute for

Human Development, Berlin, Germany (MPIB). Participants were right-handed, as assessed with a modified version of the Edinburgh Handedness Inventory [78], and had normal or corrected-to-normal vision. Participants reported to be in good health with no known history of neurological or psychiatric incidences, and were paid for their participation (10 € per hour). All older adults had Mini Mental State Examination (MMSE) [79, 80] scores above 25. All participants gave written informed consent according to the institutional guidelines of the Deutsche Gesellschaft für Psychologie (DGPS) ethics board, which approved the study.

Participants were seated at a distance of 80 cm in front of a 60 Hz LCD monitor in an acoustically and electrically shielded chamber. Following electrode placement, participants were instructed to rest for 3 minutes with their eyes open and closed, respectively. During the eyes open interval, subjects were instructed to fixate on a centrally presented fixation cross. An auditory beep indicated to the subjects when to close their eyes. Only data from the eyes open resting state were analyzed here. EEG was continuously recorded from 64 active (Ag/AgCl) electrodes using BrainAmp amplifiers (Brain Products GmbH, Gilching, Germany). Sixty scalp electrodes were arranged within an elastic cap (EASYCAP GmbH, Herrsching, Germany) according to the 10% system [81], with the ground placed at AFz. To monitor eye movements, two electrodes were placed on the outer canthi (horizontal EOG) and one electrode below the left eye (vertical EOG). During recording, all electrodes were referenced to the right mastoid electrode, while the left mastoid electrode was recorded as an additional channel. Online, signals were digitized at a sampling rate of 1 kHz.

Preprocessing and analysis of EEG data were conducted with the FieldTrip toolbox [82] and using custom-written MATLAB (The MathWorks Inc., Natick, MA, USA) code. Offline, EEG data were filtered using a 4th order Butterworth filter with a pass-band of 0.2 to 125 Hz. Subsequently, data were downsampled to 500 Hz and all channels were re-referenced to mathematically averaged mastoids. Blink, movement and heart-beat artifacts were identified using Independent Component Analysis [ICA; 83] and removed from the signal. Artifact-contaminated channels (determined across epochs) were automatically detected using (a) the FASTER algorithm [84], and by (b) detecting outliers exceeding three standard deviations of the kurtosis of the distribution of power values in each epoch within low (0.2-2 Hz) or high (30-100 Hz) frequency bands, respectively. Rejected channels were interpolated using spherical splines [85]. Subsequently, noisy epochs were likewise excluded based on FASTER and on recursive outlier detection. Finally, recordings were segmented to participant cues to open their eyes, and were epoched into non-overlapping 3 second pseudo-trials. To enhance spatial specificity, scalp current density estimates were derived via 4th order spherical splines [85] using a standard 10-05 channel layout (conductivity: 0.33 S/m; regularization: 1^-05; 14th degree polynomials).

Calculation of (modified) multi-scale sample entropy (mMSE)

MSE characterizes signal irregularity at multiple time scales by estimating sample entropy (SampEn) at each time scale of interest. A schematic of the estimation pipeline is shown in S1 Figure. The mMSE code is provided at https://github.com/LNDG/mMSE. A tutorial for computing mMSE has been published on the FieldTrip website (http://www.fieldtriptoolbox.org/example/entropy_analysis/).

Sample entropy estimation procedure. The estimation of SampEn involves counting how often patterns of *m* successive data points reoccur in time ($\boldsymbol{p^m}$) and assessing how many of those patterns remain similar when the next sample *m*+1 is added to the sequence ($\boldsymbol{p^{m+1}}$). Given that amplitude values are rarely exactly equal in physiological time series, a *similarity bound* defines which individual data points are considered similar. This step discretizes the data and allows to compare data patterns rather than exact data values. The similarity bound is defined as a proportion *r* of the time series standard deviation (*SD*; i.e., square root of signal variance) to normalize the estimation of sample entropy for total signal variation. That is, for any data point *k*, all data points within $k \pm r \times SD$ are by definition equal to *k,* which forms the basis for assessing sequence patterns. SampEn is finally given as the natural log of $\boldsymbol{p^m}(r)/\boldsymbol{p^{m+1}}(r)$. Consequently, high SampEn values indicate low temporal regularity as many patterns of length *m* are not repeated at length *m*+1. In our applications, *m* was set to 2 and r was set to .5, in line with prior recommendations [9] and EEG applications [23, 38, 86].

Multi-scale signal derivation procedure. To extend sample entropy to multiple time scales, MSE 'coarse-grains' the original time series for multiple scale factors $\boldsymbol{\tau}$ (here 1 to 42, where 1 refers to the original signal). The 'Original' MSE method [7, 8] averages time points within non-overlapping time bins (i.e., 'point averaging'). Such point averaging is equivalent to a low-pass finite-impulse response (FIR) filter, which can introduce aliasing however [29, 87] and constrains the specificity towards increasingly slow signals, while not allowing specificity to fast dynamics or any particular frequency range of interest. To implement control over the scale-wise filter direction and to reduce aliasing, we applied either low- [27, 29, 87], high-, or band-pass filters at each scale factor. The low-pass cut-off was defined as LP = $\frac{\mathbf{1}}{\boldsymbol{scale}} * \boldsymbol{nyquist}$ and was implemented using a 6th order Butterworth filter. Similarly, the high-pass cut-off was defined as HP = $\frac{\mathbf{1}}{\boldsymbol{scale+1}} * \boldsymbol{nyquist}$, implemented via 6th order Butterworth filters. Note that these cut-offs describe the upper and lower frequency bounds at each time scale, respectively. Finally, band-pass filters were applied to obtain narrowband estimates by sequentially applying Chebyshev Type I low- and high-pass filters (4th order with passband ripple of 1dB; chosen to achieve a fast filter roll-off), thus ensuring that each scale captured frequency-specific information. The passband was defined as BP = $\boldsymbol{LP}$ +- 0.05*$\mathbf{LP}$. To avoid pronounced passband ripple for broad passbands, 10th order Butterworth filters replaced the Chebyshev filters at scales where the passband was larger than 0.5*Nyquist. At scale 1, only a high-pass 10th order Butterworth filter was applied as the sampling rate of the signal set the upper (Nyquist) frequency bound. These settings were chosen to optimize the pass-through of signals within the pass-band and the attenuation of signals outside the pass-band. Two-pass filtering using MATLAB's filtfilt function was applied to achieve zero-phase delay. S4 Figure shows the spectral attenuation properties [88] of the filters. To avoid edge artefacts, input signals were symmetrically mean-padded with half the pseudo-trial duration (i.e., 1500 ms). After filtering, we implemented a point-skipping procedure to down-sample scale-wise signals (see S1 Figure). Since point-skipping allows for increasing starting point permutations *k* for increasing scale factors $\boldsymbol{\tau}$, we counted patterns separately for each starting point *k*, summed the counts of pattern matches and non-matches across them, and computed sample entropy based on the summed counts as described above: $\mathbf{MSE(x, \tau, m, r)} = \boldsymbol{ln}(\frac{\sum_{k=1}^{\tau} \boldsymbol{p^m}}{\sum_{k=1}^{\tau} \boldsymbol{p^{m+1}}})$. This implementation is equivalent

855 to "refined composite MSE" [89] and can improve the stability of entropy results for short or
856 noisy signals [27, 89]. Note that no point skipping was performed in the 'high-pass'
857 implementation to avoid low-pass filtering. As a result, the signals at increasing scale factors
858 remained at the original sampling rate. To alleviate computational cost, scale factors were
859 sampled in step sizes of 3 for empirical data (only for the 'high-pass' implementation) and later
860 spline-interpolated. An adapted version of MSE calculations was used for all settings [90], in
861 which scale-wise entropy was estimated across discontinuous data segments. The estimation of
862 scale-wise entropy across trials allows for reliable estimation of coarse-scale entropy without
863 requiring long, continuous signals, while quickly converging with estimates from continuous
864 segments [90].

865 **Multi-scale calculation of similarity bounds.** Following scale-specific filtering, all
866 implementations re-calculated sample entropy for the scale-specific signal. Crucially, in
867 'Original' applications [7, 8], the *similarity bound* is calculated only once from the original
868 broadband signal. As a result of filtering, the scale-wise signal SD decreases relative to the
869 global, scale-invariant similarity bound [25]. To overcome this limitation, we recomputed the
870 similarity bound for each scale factor, thereby normalizing MSE with respect to changes in
871 overall time series variation at each scale (.5 x SD of scale-wise signal).

872 **Scale factor notation.** As the interpretation of estimates at each scale is bound to the scale-
873 wise spectral content, our Figures indicate spectral bounds of the scale-wise signals alongside
874 the scale factor as follows: for the low- and band-pass implementation, we indicate the low-
875 pass frequency as calculated above as the highest resolvable (i.e., Nyquist) frequency in the
876 scale-specific signal. Likewise, for the high-pass implementation, we indicate the high-pass
877 limit as the lowest resolvable frequency in the scale-specific signal. In the main text, we refer
878 to higher scale factors as 'coarser' scales' and lower scale factors as 'finer' scales, in line with
879 the common use in the literature. Note that the sampling rate of the simulated data was 250 Hz,
880 whereas the empirical data had a sampling rate of 500 Hz.

881 **Calculation of power spectral density (PSD)**

882 Power spectral density estimates were computed by means of a Fast Fourier Transform
883 (FFT) over 3 second pseudo-trials for 41 logarithmically spaced frequencies between 2 and 64
884 Hz (employing a Hanning-taper; segments zero-padded to 10 seconds) and subsequently
885 averaged. Spectral power was $\log_{10}$-transformed to render power values more normally
886 distributed across subjects. Power spectral density (PSD) slopes were derived by linearly
887 regressing power values on log-transformed frequencies. The spectral range from 7-13 Hz was
888 excluded from the background fit to exclude a bias by the narrowband alpha peak [32, 41].

889 **Detection of single-trial spectral events**

890 Spectral power, even in the narrowband case, is unspecific to the occurrence of
891 systematic rhythmic events as it also characterizes periods of absent rhythmicity [e.g., 91].
892 Specifically detecting rhythmic episodes in the ongoing signal alleviates this problem, as
893 periods of absent rhythmicity are excluded. To investigate the potential relation between the

occurrence of stereotypic spectral events and narrowband entropy, we detected single-trial spectral events using the extended BOSC method [34, 92, 93] and probed their relation to individual entropy estimates. In short, this method identifies stereotypic 'rhythmic' events at the single-trial level, with the assumption that such events have significantly higher power than the 1/f background and occur for a minimum number of cycles at a particular frequency. This effectively dissociates narrowband spectral peaks from the arrhythmic background spectrum. Here, we used a one cycle threshold during detection, while defining the power threshold as the 95th percentile above the individual background power. A 5-cycle wavelet was used to provide the time-frequency transformations for 49 logarithmically-spaced center frequencies between 1 and 64 Hz. Rhythmic episodes were detected as described in [34]. Following the detection of spectral events, the rate of spectral episodes longer than 3 cycles was computed by counting the number of episodes with a mean frequency that fell in a moving window of 3 adjacent center frequencies. This produced a channel-by-frequency representation of spectral event rates, which were the basis for subsequent significance testing. Event rates and statistical results were averaged within frequency bins from 8-12 Hz (alpha) and 14-20 Hz (beta) to assess relations to narrowband entropy and for the visualization of topographies. To visualize the stereotypic depiction of single-trial alpha and beta events, the original time series were time-locked to the trough of individual spectral episodes and averaged across events [c.f., 43]. More specifically, the trough was chosen to be the local minimum during the spectral episode that was closest to the maximum power of the wavelet-transformed signal. To better estimate the local minimum, the signal was low-pass filtered at 25 Hz for alpha and bandpass-filtered between 10 and 25 Hz for beta using a 6th order Butterworth filter. A post-hoc duration threshold of one cycle was used for the visualization of beta events, whereas a three-cycle criterion was used to visualize alpha events. Alpha and beta events were visualized at channels POz and Cz, respectively.

Statistical analyses

Spectral power and entropy were compared across age groups within condition by means of independent samples t-tests; cluster-based permutation tests [94] were performed to control for multiple comparisons. Initially, a clustering algorithm formed clusters based on significant t-tests of individual data points ($p < .05$, two-sided; cluster entry threshold) with the spatial constraint of a cluster covering a minimum of three neighboring channels. Then, the significance of the observed cluster-level statistic, based on the summed t-values within the cluster, was assessed by comparison to the distribution of all permutation-based cluster-level statistics. The final cluster p-value that we report in all Figs was assessed as the proportion of 1000 Monte Carlo iterations in which the cluster-level statistic was exceeded. Cluster significance was indicated by p-values below .025 (two-sided cluster significance threshold). Effect sizes for MSE age differences with different filter settings were computed on the basis of the cluster results in the 'Original' version. This was also the case for analyses of partial correlations. Raw MSE values were extracted from channels with indicated age differences at the initial three scales 1-3 (>65 Hz) for fine MSE and scales 39-41 (<6.5 Hz) for coarse MSE. R^2 was calculated based on the t-values of an unpaired t-test: $R^2 = \frac{t^2}{t^2+df}$ [95]. The measure describes the variance in the age difference explained by the measure of interest, with the square root being identical to Pearson's correlation coefficient between continuous individual values

and binary age group. Effect sizes were compared using the r-to-z-transform and a successive comparison of the z-value difference against zero: $Z_{Diff} = \frac{z1-z2}{sqrt(\frac{1}{N1-3}+\frac{1}{N2-3})}$ [96]. Unmasked t-values are presented in support of the assessment of raw statistics in our data [97].

Acknowledgements

We thank our research assistants and participants for their contributions to the present work.

Supporting information

S1 File. Systematic literature search assessing the prevalence of global similarity bounds.

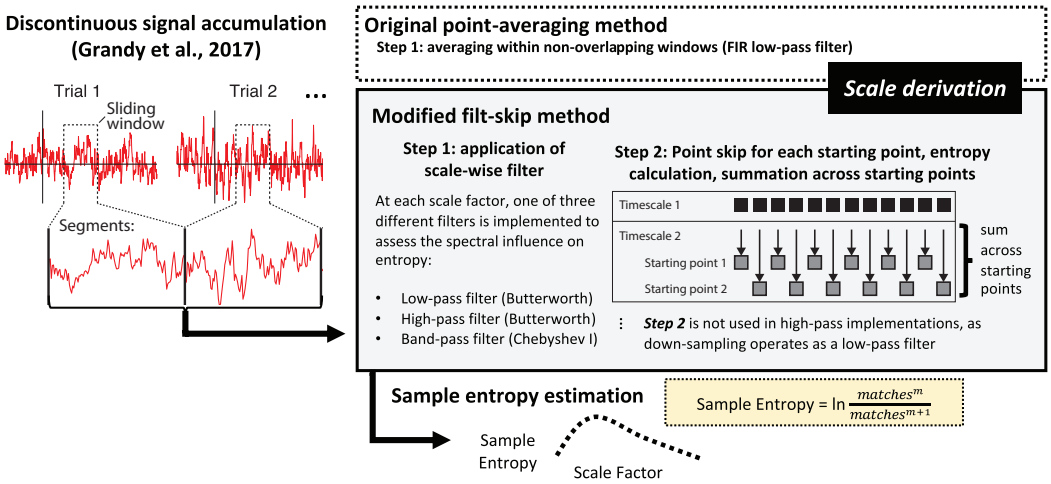

S1 Figure. Overview of modified (mMSE) adaptations. First, mMSE uses data aggregation across (here: pseudo-) trials to allow the estimation of coarse scales also from sparse neuroimaging data [90]. These aggregated signals are then filtered at each scale prior to sample entropy calculation. The 'Original' implementation uses 'point averaging' for different scale factors, which is equivalent to a FIR low-pass filter. In adapted applications, we used a two-step implementation, which we refer to as 'filt-skip', which first applies a scale-wise low-, high- or band-pass filter, and then performs point skipping to down-sample the resulting signals. Finally, the sample entropy of these signals is similarly assessed using the sample entropy algorithm, which results in multiscale entropy estimates. Figure adapted with permission from [70].

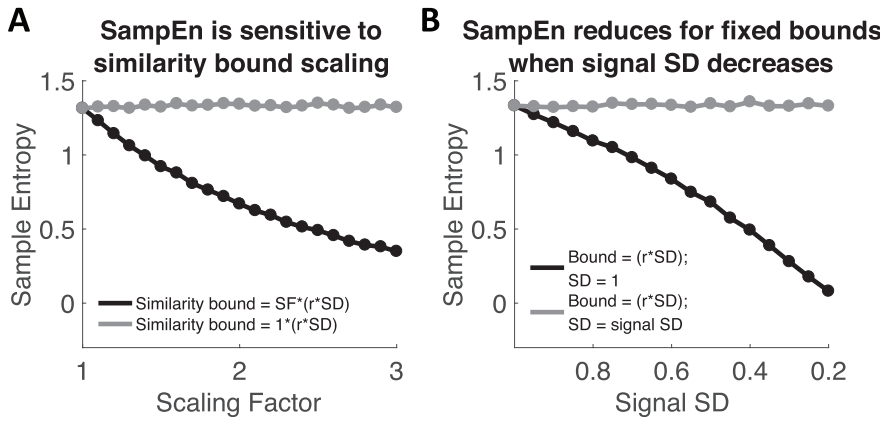

S2 Figure. Liberal similarity bounds reduce sample entropy in simulations. (**A**) The plot shows the sample entropy of simulated white noise signals with constant signal standard deviation (SD) of 1, but varying similarity bounds. We denote this as a function of a scaling factor (SF) to highlight that such variation may arise from either variation in r, SD or both. Note that the r parameter is usually fixed and the SD matches the signal SD (gray line), thus normalizing total signal variance. However, when the similarity bound systematically increases relative to the signal SD, entropy estimates progressively decrease (black line). (**B**) A similar scenario applies when fixed and

large bounds are applied to signals of decreasing variance, as is the case across MSE time scales due to scale-wise filtering (Fig 2). Whereas no bias is observed when scale-wise signal SD is used for the calculation of similarity bounds (grey line), entropy estimates systematically decrease when the SD of the original signal are used (black line). Hence, the mismatched similarity bounds introduced entropy decreases although no changes to the structure of the (here white noise) signals were introduced.

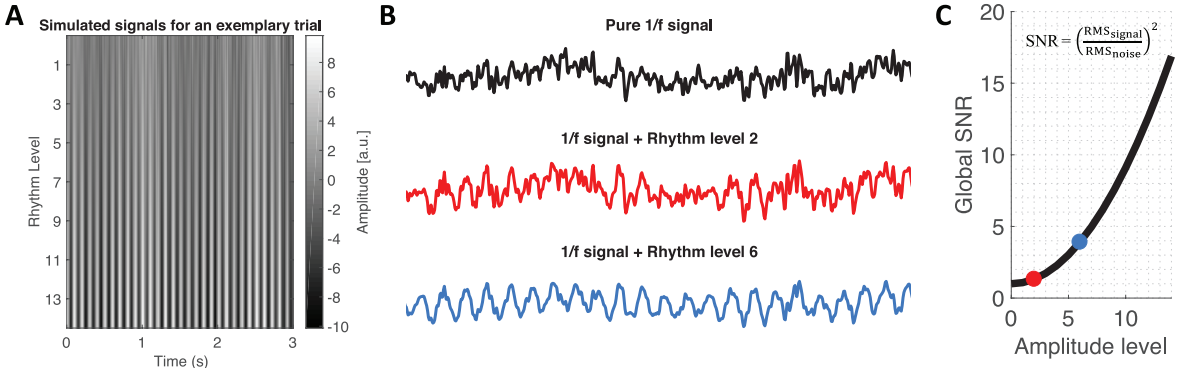

S3 Figure. Examples of simulated rhythmicity projected into pink noise. (A) Top-down view of time-series from an exemplary simulated trial for a pure 1/f signal pink noise signal and at different magnitudes of added alpha rhythmicity. **(B)** Exemplary time series in 2D view. The red time series indicates an example time series for the level of rhythmicity shown in Fig 5. (**C**) Simulated SNR as a function of amplitude level. The dots indicate SNR for the levels depicted in panel B.

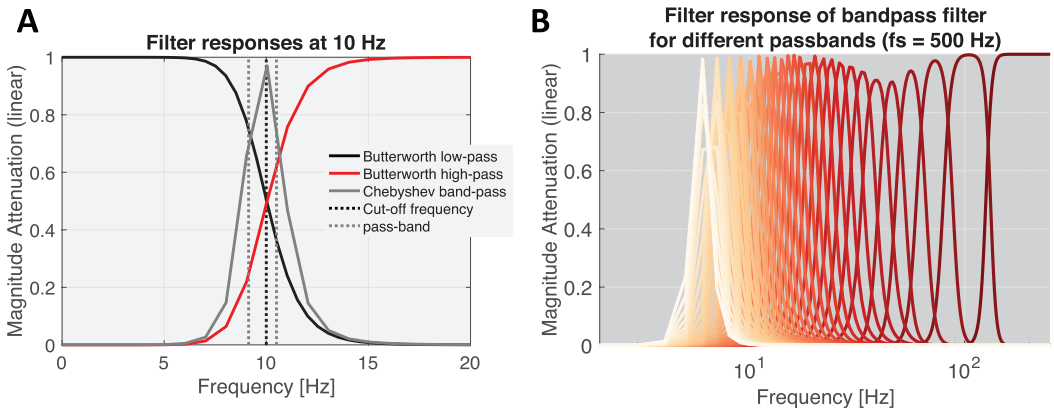

S4 Figure. Filter magnitude responses. (A) Filter magnitude responses at 10 Hz. Note that magnitude responses have been squared due to two-pass filtering to achieve zero-phase offsets. (**B**) Filter magnitudes of Bandpass filters (3rd order type I Chebyshev filter with 1dB passband ripple) at different time scales (red-to-orange indicating fine-to-coarse time scales). Note that only a high-pass filter (6th order Butterworth filter) is applied at the first scale.

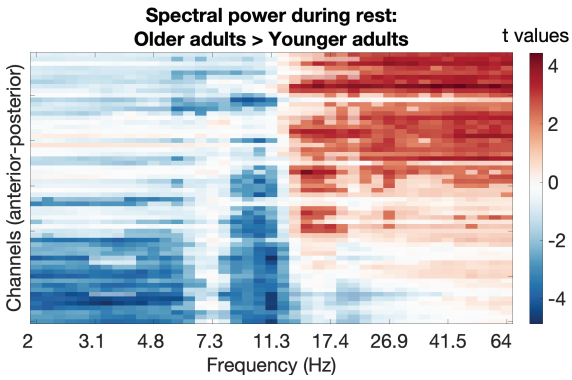

S5 Figure. T-values for age group differences in spectral power (OA > YA). Statistical significance ($p < .05$) was assessed by means of cluster-based permutation tests and is indicated via opacity.

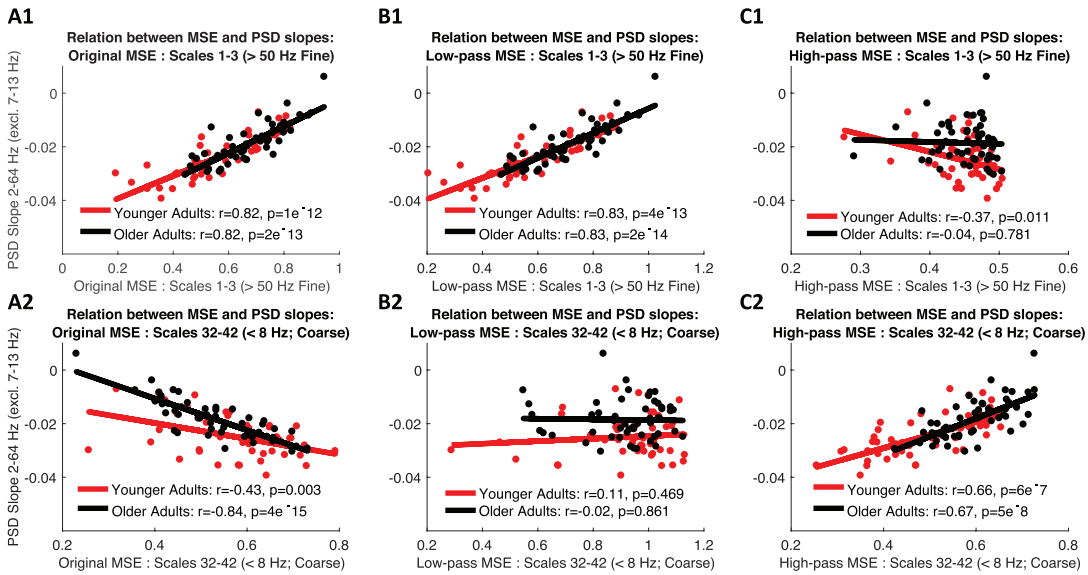

S6 Figure. Methods- and scale-dependent associations between sample entropy and PSD slopes. 'Original' settings indicate a strong positive association at fine scales (A1) that turns negative at coarse scales (A2), likely due to coarse-scale biases by the scale-invariant similarity criterion. In line with this notion, scale-wise adaptation of thresholds retains the fine-scale effect (B1), while abolishing the coarse-scale inversion (B2). Crucially, the entropy of exclusively high-frequency signals does not positively relate to PSD slopes (C1), whereas the association reemerges once slow fluctuations are added into the signal (C2).

Additional Information

Data availability

Raw empirical data is provided at https://osf.io/q3vxm/. Code used to produce simulations, empirical analyses and figures is provided at https://git.mpib-berlin.mpg.de/LNDG/rhythms_entropy. The code implementing the mMSE algorithm is available from https://github.com/LNDG/mMSE.

Funding

This study was conducted within the 'Lifespan Neural Dynamics Group' within the Max Planck UCL Centre for Computational Psychiatry and Ageing Research in the Max Planck Institute for Human Development (MPIB) in Berlin, Germany. DDG and NAK were supported by an Emmy Noether Programme grant (to DDG) from the German Research Foundation, and by the Max Planck UCL Centre for Computational Psychiatry and Ageing Research. JQK is a pre-doctoral fellow supported by the International Max Planck Research School on Computational Methods in Psychiatry and Ageing Research (IMPRS COMP2PSYCH). The participating institutions are the Max Planck Institute for Human Development, Berlin, Germany, and University College London, London, UK. For more information, see https://www.mps-ucl-centre.mpg.de/en/comp2psych.

Competing interests

The authors declare that there are no conflicts of interest.

Author contributions

Conceptualization – JQK, DDG, NAK
Data Curation – JQK, NAK
Formal Analysis – JQK
Funding Acquisition – DDG
Investigation – JQK, NAK, DDG
Methodology – JQK, NAK, DDG
Project Administration – JQK, DDG
Resources – NAK, DDG
Software – JQK, NAK
Supervision - DDG
Validation – JQK
Visualization – JQK
Writing – Original Draft Preparation – JQK
Writing – Review & Editing – JQK, NAK, DDG

References

1. Buzsaki G, Draguhn A. Neuronal oscillations in cortical networks. Science. 2004;304(5679):1926-9. doi: 10.1126/science.1099745. PubMed PMID: WOS:000222241600031.
2. Wang XJ. Neurophysiological and computational principles of cortical rhythms in cognition. Physiol Rev. 2010;90(3):1195-268. Epub 2010/07/29. doi: 10.1152/physrev.00035.2008. PubMed PMID: 20664082; PubMed Central PMCID: PMCPMC2923921.
3. Breakspear M. Dynamic models of large-scale brain activity. Nat Neurosci. 2017;20(3):340-52. doi: 10.1038/nn.4497. PubMed PMID: WOS:000394920400007.
4. Vakorin VA, McIntosh AR. Mapping the Multiscale Information Content of Complex Brain Signals. Comput Neurosci-Mit. 2012:183-208. PubMed PMID: WOS:000315291000011.
5. Stam CJ. Nonlinear dynamical analysis of EEG and MEG: review of an emerging field. Clin Neurophysiol. 2005;116(10):2266-301. Epub 2005/08/24. doi: 10.1016/j.clinph.2005.06.011. PubMed PMID: 16115797.
6. Garrett DD, Samanez-Larkin GR, MacDonald SW, Lindenberger U, McIntosh AR, Grady CL. Moment-to-moment brain signal variability: a next frontier in human brain mapping? Neurosci Biobehav Rev. 2013;37(4):610-24. Epub 2013/03/06. doi: 10.1016/j.neubiorev.2013.02.015. PubMed PMID: 23458776; PubMed Central PMCID: PMCPMC3732213.
7. Costa M, Goldberger AL, Peng CK. Multiscale entropy analysis of complex physiologic time series. Phys Rev Lett. 2002;89(6). doi: 10.1103/PhysRevLett.89.068102. PubMed PMID: WOS:000177009600047.
8. Costa M, Goldberger AL, Peng CK. Multiscale entropy analysis of biological signals. Phys Rev E. 2005;71(2). doi: 10.1103/PhysRevE.71.021906. PubMed PMID: WOS:000228245700047.
9. Richman JS, Moorman JR. Physiological time-series analysis using approximate entropy and sample entropy. Am J Physiol-Heart C. 2000;278(6):H2039-H49. PubMed PMID: WOS:000087573500038.
10. Bruce EN, Bruce MC, Vennelaganti S. Sample Entropy Tracks Changes in Electroencephalogram Power Spectrum With Sleep State and Aging. J Clin Neurophysiol. 2009;26(4):257-66. doi: 10.1097/WNP.0b013e3181b2f1e3. PubMed PMID: WOS:000268746000007.
11. Jaworska N, Wang HY, Smith DM, Blier P, Knott V, Protzner AB. Pre-treatment EEG signal variability is associated with treatment success in depression. Neuroimage-Clin. 2018;17:368-77. doi: 10.1016/j.nicl.2017.10.035. PubMed PMID: WOS:000426180300040.
12. McIntosh AR, Vakorin V, Kovacevic N, Wang H, Diaconescu A, Protzner AB. Spatiotemporal Dependency of Age-Related Changes in Brain Signal Variability. Cereb Cortex. 2014;24(7):1806-17. doi: 10.1093/cercor/bht030. PubMed PMID: WOS:000338110900010.
13. Miskovic V, MacDonald KJ, Rhodes LJ, Cote KA. Changes in EEG multiscale entropy and power-law frequency scaling during the human sleep cycle. Hum Brain

Mapp. 2019;40(2):538-51. doi: 10.1002/hbm.24393. PubMed PMID: WOS:000460481300014.

14. Wang H, McIntosh AR, Kovacevic N, Karachalios M, Protzner AB. Age-related Multiscale Changes in Brain Signal Variability in Pre-task versus Post-task Resting-state EEG. J Cogn Neurosci. 2016;28(7):971-84. Epub 2016/03/05. doi: 10.1162/jocn_a_00947. PubMed PMID: 26942319.

15. Sleimen-Malkoun R, Perdikis D, Muller V, Blanc JL, Huys R, Temprado JJ, et al. Brain Dynamics of Aging: Multiscale Variability of EEG Signals at Rest and during an Auditory Oddball Task(1,2,3). Eneuro. 2015;2(3). doi: 10.1523/ENEURO.0067-14.2015. PubMed PMID: WOS:000218581400012.

16. Werkle-Bergner M, Grandy TH, Chicherio C, Schmiedek F, Lovden M, Lindenberger U. Coordinated within-Trial Dynamics of Low-Frequency Neural Rhythms Controls Evidence Accumulation. J Neurosci. 2014;34(25):8519-28. doi: 10.1523/Jneurosci.3801-13.2014. PubMed PMID: WOS:000338449200014.

17. Yang AC, Wang SJ, Lai KL, Tsai CF, Yang CH, Hwang JP, et al. Cognitive and neuropsychiatric correlates of EEG dynamic complexity in patients with Alzheimer's disease. Prog Neuro-Psychoph. 2013;47:52-61. doi: 10.1016/j.pnpbp.2013.07.022. PubMed PMID: WOS:000326682300009.

18. Takahashi T, Cho RY, Mizuno T, Kikuchi M, Murata T, Takahashi K, et al. Antipsychotics reverse abnormal EEG complexity in drug-naive schizophrenia: A multiscale entropy analysis. Neuroimage. 2010;51(1):173-82. doi: 10.1016/j.neuroimage.2010.02.009. PubMed PMID: WOS:000276480200018.

19. Mejias JF, Murray JD, Kennedy H, Wang XJ. Feedforward and feedback frequency-dependent interactions in a large-scale laminar network of the primate cortex. Sci Adv. 2016;2(11). doi: 10.1126/sciadv.1601335. PubMed PMID: WOS:000391267800032.

20. Buzsaki G, Logothetis N, Singer W. Scaling Brain Size, Keeping Timing: Evolutionary Preservation of Brain Rhythms. Neuron. 2013;80(3):751-64. doi: 10.1016/j.neuron.2013.10.002. PubMed PMID: WOS:000326609900019.

21. von Stein A, Sarnthein J. Different frequencies for different scales of cortical integration: from local gamma to long range alpha/theta synchronization. Int J Psychophysiol. 2000;38(3):301-13. doi: 10.1016/S0167-8760(00)00172-0. PubMed PMID: WOS:000165915000009.

22. Fries P. Neuronal Gamma-Band Synchronization as a Fundamental Process in Cortical Computation. Annu Rev Neurosci. 2009;32:209-24. doi: 10.1146/annurev.neuro.051508.135603. PubMed PMID: WOS:000268504100009.

23. Courtiol J, Perdikis D, Petkoski S, Muller V, Huys R, Sleimen-Malkoun R, et al. The multiscale entropy: Guidelines for use and interpretation in brain signal analysis. J Neurosci Meth. 2016;273:175-90. doi: 10.1016/j.jneumeth.2016.09.004. PubMed PMID: WOS:000387195800017.

24. Costa M, Goldberger AL, Peng CK. Comment on "Multiscale entropy analysis of complex physiologic time series" - Reply. Phys Rev Lett. 2004;92(8). doi: 10.1103/PhysRevLett.92.089804. PubMed PMID: WOS:000189266100069.

25. Nikulin VV, Brismar T. Comment on "Multiscale entropy analysis of complex physiologic time series". Phys Rev Lett. 2004;92(8). doi: 10.1103/PhysRevLett.92.089803. PubMed PMID: WOS:000189266100068.

26. Shafiei G, Zeighami Y, Clark CA, Coull JT, Nagano-Saito A, Leyton M, et al. Dopamine Signaling Modulates the Stability and Integration of Intrinsic Brain Networks. Cereb Cortex. 2019;29(1):397-409. doi: 10.1093/cercor/bhy264. PubMed PMID: WOS:000459518500030.
27. Azami H, Escudero J. Coarse-Graining Approaches in Univariate Multiscale Sample and Dispersion Entropy. Entropy. 2018;20(2). doi: 10.3390/e20020138. PubMed PMID: WOS:000426793900061.
28. Miskovic V, Owens M, Kuntzelman K, Gibb BE. Charting moment-to-moment brain signal variability from early to late childhood. Cortex. 2016;83:51-61. Epub 2016/08/02. doi: 10.1016/j.cortex.2016.07.006. PubMed PMID: 27479615; PubMed Central PMCID: PMCPMC5042835.
29. Valencia JF, Porta A, Vallverdu M, Claria F, Baranowski R, Orlowska-Baranowska E, et al. Refined Multiscale Entropy: Application to 24-h Holter Recordings of Heart Period Variability in Healthy and Aortic Stenosis Subjects. Ieee T Bio-Med Eng. 2009;56(9):2202-13. doi: 10.1109/Tbme.2009.2021986. PubMed PMID: WOS:000269154100008.
30. Buzsaki G, Mizuseki K. The log-dynamic brain: how skewed distributions affect network operations. Nat Rev Neurosci. 2014;15(4):264-78. doi: 10.1038/nrn3687. PubMed PMID: WOS:000333256600012.
31. He BYJ. Scale-free brain activity: past, present, and future. Trends Cogn Sci. 2014;18(9):480-7. doi: 10.1016/j.tics.2014.04.003. PubMed PMID: WOS:000341613000010.
32. Waschke L, Wostmann M, Obleser J. States and traits of neural irregularity in the age-varying human brain. Sci Rep-Uk. 2017;7. doi: 10.1038/s41598-017-17766-4. PubMed PMID: WOS:000417689400005.
33. Haller M, Donoghue T, Peterson E, Varma P, Sebastian P, Gao R, et al. Parameterizing neural power spectra. bioRxiv. 2018.
34. Kosciessa JQ, Grandy TH, Garrett DD, Werkle-Bergner M. Single-trial characterization of neural rhythms: Potential and challenges. Neuroimage. 2019:116331. doi: https://doi.org/10.1016/j.neuroimage.2019.116331.
35. Lopes da Silva F. EEG and MEG: relevance to neuroscience. Neuron. 2013;80(5):1112-28. Epub 2013/12/10. doi: 10.1016/j.neuron.2013.10.017. PubMed PMID: 24314724.
36. Park JH, Kim S, Kim CH, Cichocki A, Kim K. Multiscale entropy analysis of EEG from patients under different pathological conditions. Fractals. 2007;15(4):399-404. doi: 10.1142/S0218348x07003691. PubMed PMID: WOS:000252021600010.
37. McIntosh AR. Neurocognitive Aging and Brain Signal Complexity. Oxford University Press; 2019.
38. McIntosh AR, Kovacevic N, Itier RJ. Increased Brain Signal Variability Accompanies Lower Behavioral Variability in Development. Plos Comput Biol. 2008;4(7). doi: 10.1371/journal.pcbi.1000106. PubMed PMID: WOS:000260039300027.
39. Leirer VM, Wienbruch C, Kolassa S, Schlee W, Elbert T, Kolassa IT. Changes in cortical slow wave activity in healthy aging. Brain Imaging Behav. 2011;5(3):222-8. doi: 10.1007/s11682-011-9126-3. PubMed PMID: WOS:000293498500007.

40. Vlahou EL, Thurm F, Kolassa IT, Schlee W. Resting-state slow wave power, healthy aging and cognitive performance. Sci Rep-Uk. 2014;4. doi: 10.1038/srep05101. PubMed PMID: WOS:000336516800002.
41. Voytek B, Kramer MA, Case J, Lepage KQ, Tempesta ZR, Knight RT, et al. Age-Related Changes in 1/f Neural Electrophysiological Noise. J Neurosci. 2015;35(38):13257-65. doi: 10.1523/Jneurosci.2332-14.2015. PubMed PMID: WOS:000363660200027.
42. Hipp JF, Siegel M. Dissociating neuronal gamma-band activity from cranial and ocular muscle activity in EEG. Front Hum Neurosci. 2013;7. doi: 10.3389/fnhum.2013.00338. PubMed PMID: WOS:000321588600001.
43. Sherman MA, Lee S, Law R, Haegens S, Thorn CA, Hamalainen MS, et al. Neural mechanisms of transient neocortical beta rhythms: Converging evidence from humans, computational modeling, monkeys, and mice. P Natl Acad Sci USA. 2016;113(33):E4885-E94. doi: 10.1073/pnas.1604135113. PubMed PMID: WOS:000381399200018.
44. Shin H, Law R, Tsutsui S, Moore CI, Jones SR. The rate of transient beta frequency events predicts behavior across tasks and species. Elife. 2017;6. doi: 10.7554/eLife.29086. PubMed PMID: WOS:000414984800001.
45. Waschke L, Tune S, Obleser J. Local cortical desynchronization and pupil-linked arousal differentially shape brain states for optimal sensory performance. Elife. 2019;8. Epub 2019/12/11. doi: 10.7554/eLife.51501. PubMed PMID: 31820732.
46. Contreras D, Steriade M. Synchronization of low-frequency rhythms in corticothalamic networks. Neuroscience. 1997;76(1):11-24. PubMed PMID: WOS:A1997VY25600003.
47. Harris KD, Thiele A. Cortical state and attention. Nat Rev Neurosci. 2011;12(9):509-23. doi: 10.1038/nrn3084. PubMed PMID: WOS:000294049200013.
48. Marguet SL, Harris KD. State-Dependent Representation of Amplitude-Modulated Noise Stimuli in Rat Auditory Cortex. J Neurosci. 2011;31(17):6414-20. doi: 10.1523/Jneurosci.5773-10.2011. PubMed PMID: WOS:000289934600018.
49. Gao R, Peterson EJ, Voytek B. Inferring synaptic excitation/inhibition balance from field potentials. Neuroimage. 2017;158:70-8. doi: 10.1016/j.neuroimage.2017.06.078. PubMed PMID: WOS:000411450600008.
50. Peterson EJ, Rosen BQ, Campbell AM, Belger A, Voytek B. 1/f neural noise is a better predictor of schizophrenia than neural oscillations. bioRxiv. 2018.
51. Sheehan TC, Sreekumar V, Inati SK, Zaghloul KA. Signal Complexity of Human Intracranial EEG Tracks Successful Associative-Memory Formation across Individuals. J Neurosci. 2018;38(7):1744-55. doi: 10.1523/Jneurosci.2389-17.2017. PubMed PMID: WOS:000424987700012.
52. Kaffashi F, Foglyano R, Wilson CG, Loparo KA. The effect of time delay on Approximate & Sample Entropy calculations. Physica D. 2008;237(23):3069-74. doi: 10.1016/j.physd.2008.06.005. PubMed PMID: WOS:000261463000010.
53. Misic B, Vakorin VA, Paus T, McIntosh AR. Functional embedding predicts the variability of neural activity. Front Syst Neurosci. 2011;5:90. Epub 2011/12/14. doi: 10.3389/fnsys.2011.00090. PubMed PMID: 22164135; PubMed Central PMCID: PMCPMC3225043.

54. Deco G, Jirsa VK, McIntosh AR. Resting brains never rest: computational insights into potential cognitive architectures. Trends Neurosci. 2013;36(5):268-74. Epub 2013/04/09. doi: 10.1016/j.tins.2013.03.001. PubMed PMID: 23561718.
55. Deco G, Jirsa VK, McIntosh AR. Emerging concepts for the dynamical organization of resting-state activity in the brain. Nat Rev Neurosci. 2011;12(1):43-56. Epub 2010/12/21. doi: 10.1038/nrn2961. PubMed PMID: 21170073.
56. Ishii R, Canuet L, Aoki Y, Hata M, Iwase M, Ikeda S, et al. Healthy and Pathological Brain Aging: From the Perspective of Oscillations, Functional Connectivity, and Signal Complexity. Neuropsychobiology. 2017;75(4):151-61. Epub 2018/02/22. doi: 10.1159/000486870. PubMed PMID: 29466802.
57. Caplan JB, Bottomley M, Kang P, Dixon RA. Distinguishing rhythmic from non-rhythmic brain activity during rest in healthy neurocognitive aging. Neuroimage. 2015;112:341-52. Epub 2015/03/15. doi: 10.1016/j.neuroimage.2015.03.001. PubMed PMID: 25769279; PubMed Central PMCID: PMCPMC4408255.
58. Rossiter HE, Davis EM, Clark EV, Boudrias MH, Ward NS. Beta oscillations reflect changes in motor cortex inhibition in healthy ageing. Neuroimage. 2014;91:360-5. Epub 2014/01/21. doi: 10.1016/j.neuroimage.2014.01.012. PubMed PMID: 24440529; PubMed Central PMCID: PMCPMC3988925.
59. Cole S, Voytek B. Cycle-by-cycle analysis of neural oscillations. bioRxiv. 2018.
60. Heisz JJ, Shedden JM, McIntosh AR. Relating brain signal variability to knowledge representation. Neuroimage. 2012;63(3):1384-92. doi: 10.1016/j.neuroimage.2012.08.018. PubMed PMID: WOS:000310379100040.
61. Lippe S, Kovacevic N, McIntosh AR. Differential maturation of brain signal complexity in the human auditory and visual system. Front Hum Neurosci. 2009;3. doi: 10.3389/neuro.09.048.2009. PubMed PMID: WOS:000274619300008.
62. Mizuno T, Takahashi T, Cho RY, Kikuchi M, Murata T, Takahashi K, et al. Assessment of EEG dynamical complexity in Alzheimer's disease using multiscale entropy. Clin Neurophysiol. 2010;121(9):1438-46. doi: 10.1016/j.clinph.2010.03.025. PubMed PMID: WOS:000280555400007.
63. Szostakiwskyj JMH, Willatt SE, Cortese F, Protzner AB. The modulation of EEG variability between internally-and externally-driven cognitive states varies with maturation and task performance. Plos One. 2017;12(7). doi: 10.1371/journal.pone.0181894. PubMed PMID: WOS:000406575700098.
64. Takahashi T, Cho RY, Murata T, Mizuno T, Kikuchi M, Mizukami K, et al. Age-related variation in EEG complexity to photic stimulation: A multiscale entropy analysis. Clin Neurophysiol. 2009;120(3):476-83. doi: 10.1016/j.clinph.2008.12.043. PubMed PMID: WOS:000265772400006.
65. Carpentier SM, McCulloch AR, Brown TM, Ritter P, Wang Z, Salimpoor V, et al. Complexity matching: brain signals mirror environment information patterns during music listening and reward. bioRxiv. 2019.
66. Raja Beharelle A, Kovacevic N, McIntosh AR, Levine B. Brain signal variability relates to stability of behavior after recovery from diffuse brain injury. Neuroimage. 2012;60(2):1528-37. Epub 2012/01/21. doi: 10.1016/j.neuroimage.2012.01.037. PubMed PMID: 22261371; PubMed Central PMCID: PMCPMC3303989.

67. Catarino A, Churches O, Baron-Cohen S, Andrade A, Ring H. Atypical EEG complexity in autism spectrum conditions: A multiscale entropy analysis. Clin Neurophysiol. 2011;122(12):2375-83. doi: 10.1016/j.clinph.2011.05.004. PubMed PMID: WOS:000296583000008.
68. Misic B, Doesburg SM, Fatima Z, Vidal J, Vakorin VA, Taylor MJ, et al. Coordinated Information Generation and Mental Flexibility: Large-Scale Network Disruption in Children with Autism. Cereb Cortex. 2015;25(9):2815-27. doi: 10.1093/cercor/bhu082. PubMed PMID: WOS:000361464000042.
69. Ueno K, Takahashi T, Takahashi K, Mizukami K, Tanaka Y, Wada Y. Neurophysiological basis of creativity in healthy elderly people: A multiscale entropy approach. Clin Neurophysiol. 2015;126(3):524-31. doi: 10.1016/j.clinph.2014.06.032. PubMed PMID: WOS:000349616700015.
70. Kloosterman NA, Kosciessa JQ, Lindenberger U, Fahrenfort JJ, Garrett DD. Boosting Brain Signal Variability Underlies Liberal Shifts in Decision Bias. bioRxiv. 2019.
71. Theiler J, Eubank S, Longtin A, Galdrikian B, Farmer JD. Testing for Nonlinearity in Time-Series - the Method of Surrogate Data. Physica D. 1992;58(1-4):77-94. doi: 10.1016/0167-2789(92)90102-S. PubMed PMID: WOS:A1992JV85800006.
72. Garrett DD, Grandy TH, Werkle-Bergner M. The neural forest and the trees: On distinguishing the variance of a brain signal from its information content. Annual Alpine Brain Imaging Meeting; Champéry, Switzerland2014.
73. Grandy TH, Garrett DD, Lindenberger U, Werkle-Bergner M. Exploring the limits of complexity measures for the analysis of age differences in neural signals. Dallas Aging and Cognition Conference; Dallas, TX, USA2013.
74. Takens F. Detecting Nonlinearities in Stationary Time Series. Int J Bifurcat Chaos. 1993;3(2):241-56. doi: 10.1142/S0218127493000192. PubMed PMID: WOS:000209750900002.
75. Kloosterman NA, de Gee JW, Werkle-Bergner M, Lindenberger U, Garrett DD, Fahrenfort JJ. Humans strategically shift decision bias by flexibly adjusting sensory evidence accumulation. Elife. 2019;8. Epub 2019/02/07. doi: 10.7554/eLife.37321. PubMed PMID: 30724733; PubMed Central PMCID: PMCPMC6365056.
76. Simpraga S, Alvarez-Jimenez R, Mansvelder HD, van Gerven JMA, Groeneveld GJ, Poil SS, et al. EEG machine learning for accurate detection of cholinergic intervention and Alzheimer's disease. Sci Rep-Uk. 2017;7. doi: 10.1038/s41598-017-06165-4. PubMed PMID: WOS:000405746500086.
77. Stoyanov M, Gunzburger M, Burkardt J. Pink noise, 1/f (alpha) noise, and their effect on solutions of differential equations. Int J Uncertain Quan. 2011;1(3):257-78. doi: 10.1615/Int.J.UncertaintyQuantification.2011003089. PubMed PMID: WOS:000209100100005.
78. Oldfield RC. The Assessment and Analysis of Handedness: The Edinburgh Inventory. Neuropsychologia. 1971;9(1):97-113. doi: 10.1016/0028-3932(71)90067-4. PubMed PMID: WOS:A1971J199600013.
79. Folstein MF, Robins LN, Helzer JE. The Mini-Mental State Examination. Arch Gen Psychiat. 1983;40(7):812-. PubMed PMID: WOS:A1983QX57000014.
80. Kessler J, Markowitsch H, Denzler P. Mini-mental-status-test (MMST). Göttingen: Beltz Test GMBH; 2000.

81. Oostenveld R, Praamstra P. The five percent electrode system for high-resolution EEG and ERP measurements. Clin Neurophysiol. 2001;112(4):713-9. doi: 10.1016/S1388-2457(00)00527-7. PubMed PMID: WOS:000168113100018.
82. Oostenveld R, Fries P, Maris E, Schoffelen JM. FieldTrip: Open Source Software for Advanced Analysis of MEG, EEG, and Invasive Electrophysiological Data. Comput Intel Neurosc. 2011. doi: 10.1155/2011/156869. PubMed PMID: WOS:000208906100004.
83. Bell AJ, Sejnowski TJ. An Information Maximization Approach to Blind Separation and Blind Deconvolution. Neural Comput. 1995;7(6):1129-59. doi: 10.1162/neco.1995.7.6.1129. PubMed PMID: WOS:A1995RZ70200001.
84. Nolan H, Whelan R, Reilly RB. FASTER: Fully Automated Statistical Thresholding for EEG artifact Rejection. J Neurosci Meth. 2010;192(1):152-62. doi: 10.1016/j.jneumeth.2010.07.015. PubMed PMID: WOS:000283477500020.
85. Perrin F, Pernier J, Bertrand O, Echallier JF. Spherical Splines for Scalp Potential and Current-Density Mapping. Electroen Clin Neuro. 1989;72(2):184-7. doi: 10.1016/0013-4694(89)90180-6. PubMed PMID: WOS:A1989T157400011.
86. Heisz JJ, McIntosh AR. Applications of EEG Neuroimaging Data: Event-related Potentials, Spectral Power, and Multiscale Entropy. Jove-Journal of Visualized Experiments. 2013;(76). doi: 10.3791/50131. PubMed PMID: WOS:000209227800013.
87. Semmlow JL. Biosignal and medical image processing: CRC press; 2008.
88. Widmann A, Schroger E, Maess B. Digital filter design for electrophysiological data - a practical approach. J Neurosci Meth. 2015;250:34-46. doi: 10.1016/j.jneumeth.2014.08.002. PubMed PMID: WOS:000356978900005.
89. Wu SD, Wu CW, Lin SG, Lee KY, Peng CK. Analysis of complex time series using refined composite multiscale entropy. Phys Lett A. 2014;378(20):1369-74. doi: 10.1016/j.physleta.2014.03.034. PubMed PMID: WOS:000335704900007.
90. Grandy TH, Garrett DD, Schmiedek F, Werkle-Bergner M. On the estimation of brain signal entropy from sparse neuroimaging data. Sci Rep-Uk. 2016;6. doi: 10.1038/srep23073. PubMed PMID: WOS:000372915300001.
91. Jones SR. When brain rhythms aren't 'rhythmic': implication for their mechanisms and meaning. Curr Opin Neurobiol. 2016;40:72-80. doi: 10.1016/j.conb.2016.06.010. PubMed PMID: WOS:000386405800012.
92. Caplan JB, Madsen JR, Raghavachari S, Kahana MJ. Distinct patterns of brain oscillations underlie two basic parameters of human maze learning. J Neurophysiol. 2001;86(1):368-80. PubMed PMID: WOS:000169955100033.
93. Whitten TA, Hughes AM, Dickson CT, Caplan JB. A better oscillation detection method robustly extracts EEG rhythms across brain state changes: The human alpha rhythm as a test case. Neuroimage. 2011;54(2):860-74. doi: 10.1016/j.neuroimage.2010.08.064. PubMed PMID: WOS:000285486000013.
94. Maris E, Oostenveld R. Nonparametric statistical testing of EEG- and MEG-data. J Neurosci Meth. 2007;164(1):177-90. doi: 10.1016/j.jneumeth.2007.03.024. PubMed PMID: WOS:000248170300019.

95. Lakens D. Calculating and reporting effect sizes to facilitate cumulative science: a practical primer for t-tests and ANOVAs. Front Psychol. 2013;4. doi: 10.3389/fpsyg.2013.00863. PubMed PMID: WOS:000331576200001.
96. Brandner FA. A test of the significance of the difference of the correlation coefficients in normal bivariate samples. Biometrika. 1933;25:102-9. doi: 10.1093/biomet/25.1-2.102. PubMed PMID: WOS:000200863000008.
97. Allen EA, Erhardt EB, Calhoun VD. Data Visualization in the Neurosciences: Overcoming the Curse of Dimensionality. Neuron. 2012;74(4):603-8. doi: 10.1016/j.neuron.2012.05.001. PubMed PMID: WOS:000304747200004.

Supplementary Information for

Standard multiscale entropy reflects spectral power at mismatched temporal scales

Julian Q. Kosciessa, Niels A. Kloosterman, and Douglas D. Garrett

Email: kosciessa@mpib-berlin.mpg.de; garrett@mpib-berlin.mpg.de

S1 Text. Systematic literature search assessing the prevalence of global similarity bounds. We performed a systematic literature search to assess the prevalence of global similarity bounds in current neuroscientific applications (heart rate variability applications are specifically marked). We searched Pubmed (https://www.ncbi.nlm.nih.gov/pubmed) with the following terms: *(MSE AND sample entropy AND EEG) OR (MSE AND brain AND variability) OR (MSE AND EEG AND variability) OR (multiscale entropy AND EEG AND variability).* We excluded any studies that did not assess multiscale entropy, including studies that were restricted to sample entropy at scale 1. In addition, we added references from the main text that were not captured by the systematic search (highlighted in grey). For MSE applications, we checked the text for a notion of how similarity bounds were computed, i.e., whether it was calculated as r*SD of the original time series or the coarse-grained time series. The following sections list the results of this qualitative review and is purely intended to characterize the prevalence of global similarity bounds, not as a qualitative judgement on the claims made in any particular paper. Our literature search revealed the following papers. The relative amount of studies with presumably global similarity bounds was as follows (39+13)/(39+13+4) = 0,928; i.e., > 90%.

<u>Scale-invariant similarity bounds (r x global SD)</u>
We chose this category, when the article contained the specific information that r was calculated from the original signal (i.e., scale-invariant).

Azami, Fernandez, and Escudero (2017)
Azami, Rostaghi, Abasolo, and Escudero (2017)
Carpentier et al. (2019)
Escudero, Abasolo, Hornero, Espino, and Lopez (2006) [but they note the issue]
Grandy, Garrett, Schmiedek, and Werkle-Bergner (2016)
Hadoush, Alafeef, and Abdulhay (2019)
Kaur et al. (2019)
M. Liu, Song, Liang, Knopfel, and Zhou (2019)
H. Liu et al. (2017) [HRV]
Lu et al. (2015)
McIntosh, Kovacevic, and Itier (2008)
Mizuno et al. (2010)
Weng et al. (2015)

#: 13

<u>Unclear, assumed scale-invariant similarity bounds (r x global SD)</u>
We chose this category, when the article did not contain any information about how r was calculated, or no reference was made to scale-specific adaptations. For many papers, Costa, Goldberger, and Peng (2002, 2005) or Richman and Moorman (2000) were cited, which use scale-invariant implementations.

Raja Beharelle, Kovacevic, McIntosh, and Levine (2012)
Bertrand et al. (2016)
Catarino, Churches, Baron-Cohen, Andrade, and Ring (2011)
Chen et al. (2015)(HRV)
Chen et al. (2018) (HRV)

Li, Chen, Li, Wang, and Liu (2016)
Chiu et al. (2015) (HRV)
Courtiol et al. (2016)
Gao, Hu, Liu, and Cao (2015)
Harati, Crowell, Huang, Mayberg, and Nemati (2019)
Harati, Crowell, Mayberg, Jun, and Nemati (2016)
Hasegawa et al. (2018)
Heisz and McIntosh (2013)
Heisz, Shedden, and McIntosh (2012)
Hu and Liang (2012) [RM]
Hussain, Saeed, Awan, and Idris (2018)
Hussain, Aziz, et al. (2018)
Jaworska et al. (2018)
Kuntzelman, Jack Rhodes, Harrington, and Miskovic (2018)
Lin et al. (2019) [BOLD]
H. Liu et al. (2018)
H. Y. Liu et al. (2018)
Q. Liu, Chen, Fan, Abbod, and Shieh (2015)
Q. Liu, Chen, Fan, Abbod, and Shieh (2017)
McIntosh et al. (2014)
Misic et al. (2015)
Misic, Vakorin, Paus, and McIntosh (2011)
Miskovic, Owens, Kuntzelman, and Gibb (2016)
Park, Kim, Kim, Cichocki, and Kim (2007)
Roldan, Molina-Pico, Cuesta-Frau, Martinez, and Crespo (2011)
Szostakiwskyj, Willatt, Cortese, and Protzner (2017)
Takahashi et al. (2009)
Takahashi et al. (2010)
Takahashi et al. (2016)
Ueno et al. (2015)
Yang et al. (2013)
H. Y. Wang, McIntosh, Kovacevic, Karachalios, and Protzner (2016)
H. Wang, Pexman, Turner, Cortese, and Protzner (2018)
Wei et al. (2014)

#: 39

<u>Scale-wise similarity bounds (r x scale-wise SD)</u>
We chose this category, when the article either specified that scale-wise recalculation of r parameters was performed, or when the description could allow that inference.

Fabris et al. (2014) [but with unclear variations in r]
Sleimen-Malkoun et al. (2015)
Valencia et al. (2009) [HRV]
Zavala-Yoe, Ramirez-Mendoza, and Cordero (2015)

#: 4

<u>Not applicable</u>
We chose this category, when multi-scale entropy was not used in the study (i.e., erroneous listing of paper).

El-Gohary, McNames, and Elsas (2008)

Erdogan, Yucel, and Akin (2014)
Fernandez, Gomez, Hornero, and Lopez-Ibor (2013)
Heunis, Aldrich, and de Vries (2016)
Hier, Jao, and Brint (1994)
Kielar et al. (2016) [BOLD MSE, single scale]
Nazari et al. (2019)
Puce, Berkovic, Cadusch, and Bladin (1994)
Sinai, Phillips, Chertkow, and Kabani (2010)
Verhaeghe, Gravel, and Reader (2010)
Xu, Cui, Hong, and Liang (2015)

Supplementary References

Azami, H., Fernandez, A., & Escudero, J. (2017). Refined multiscale fuzzy entropy based on standard deviation for biomedical signal analysis. *Med Biol Eng Comput, 55*(11), 2037-2052. doi:10.1007/s11517-017-1647-5

Azami, H., Rostaghi, M., Abasolo, D., & Escudero, J. (2017). Refined Composite Multiscale Dispersion Entropy and its Application to Biomedical Signals. *Ieee Transactions on Biomedical Engineering, 64*(12), 2872-2879. doi:10.1109/tbme.2017.2679136

Bandt, C., & Pompe, B. (2002). Permutation entropy: A natural complexity measure for time series. *Physical Review Letters, 88*(17). doi:10.1103/PhysRevLett.88.174102

Bertrand, J. A., McIntosh, A. R., Postuma, R. B., Kovacevic, N., Latreille, V., Panisset, M., . . . Gagnon, J. F. (2016). Brain Connectivity Alterations Are Associated with the Development of Dementia in Parkinson's Disease. *Brain Connectivity, 6*(3), 216-224. doi:10.1089/brain.2015.0390

Carpentier, S. M., McCulloch, A. R., Brown, T. M., Ritter, P., Wang, Z., Salimpoor, V., . . . McIntosh, A. R. (2019). Complexity matching: brain signals mirror environment information patterns during music listening and reward. *bioRxiv*.

Catarino, A., Churches, O., Baron-Cohen, S., Andrade, A., & Ring, H. (2011). Atypical EEG complexity in autism spectrum conditions: A multiscale entropy analysis. *Clinical Neurophysiology, 122*(12), 2375-2383. doi:10.1016/j.clinph.2011.05.004

Chen, C. H., Huang, P. W., Tang, S. C., Shieh, J. S., Lai, D. M., Wu, A. Y., & Jeng, J. S. (2015). Complexity of Heart Rate Variability Can Predict Stroke-In-Evolution in Acute Ischemic Stroke Patients. *Sci Rep, 5*, 17552. doi:10.1038/srep17552

Chen, C. H., Tang, S. C., Lee, D. Y., Shieh, J. S., Lai, D. M., Wu, A. Y., & Jeng, J. S. (2018). Impact of Supratentorial Cerebral Hemorrhage on the Complexity of Heart Rate Variability in Acute Stroke. *Sci Rep, 8*(1), 11473. doi:10.1038/s41598-018-29961-y

Chiu, H. C., Lin, Y. H., Lo, M. T., Tang, S. C., Wang, T. D., Lu, H. C., . . . Peng, C. K. (2015). Complexity of cardiac signals for predicting changes in alpha-waves after stress in patients undergoing cardiac catheterization. *Scientific Reports, 5*. doi:10.1038/srep13315

Costa, M., Goldberger, A. L., & Peng, C. K. (2002). Multiscale entropy analysis of complex physiologic time series. *Physical Review Letters, 89*(6). doi:10.1103/PhysRevLett.89.068102

Costa, M., Goldberger, A. L., & Peng, C. K. (2005). Multiscale entropy analysis of biological signals. *Physical Review E, 71*(2). doi:10.1103/PhysRevE.71.021906

Courtiol, J., Perdikis, D., Petkoski, S., Muller, V., Huys, R., Sleimen-Malkoun, R., & Jirsa, V. K. (2016). The multiscale entropy: Guidelines for use and interpretation in brain signal analysis. *Journal of Neuroscience Methods, 273*, 175-190. doi:10.1016/j.jneumeth.2016.09.004

El-Gohary, M., McNames, J., & Elsas, S. (2008). User-guided interictal spike detection. *Conf Proc IEEE Eng Med Biol Soc, 2008*, 821-824. doi:10.1109/iembs.2008.4649280

Erdogan, S. B., Yucel, M. A., & Akin, A. (2014). Analysis of task-evoked systemic interference in fNIRS measurements: insights from fMRI. *Neuroimage, 87*, 490-504. doi:10.1016/j.neuroimage.2013.10.024

Escudero, J., Abasolo, D., Hornero, R., Espino, P., & Lopez, M. (2006). Analysis of electroencephalograms in Alzheimer's disease patients with multiscale entropy. *Physiological Measurement, 27*(11), 1091-1106. doi:10.1088/0967-3334/27/11/004

Fabris, C., Sparacino, G., Sejling, A. S., Goljahani, A., Duun-Henriksen, J., Remvig, L. S., . . . Cobelli, C. (2014). Hypoglycemia-Related Electroencephalogram Changes Assessed by Multiscale Entropy. *Diabetes Technology & Therapeutics, 16*(10), 688-694. doi:10.1089/dia.2013.0331

Fernandez, A., Gomez, C., Hornero, R., & Lopez-Ibor, J. J. (2013). Complexity and schizophrenia. *Prog Neuropsychopharmacol Biol Psychiatry, 45*, 267-276. doi:10.1016/j.pnpbp.2012.03.015

Gao, J., Hu, J., Liu, F., & Cao, Y. (2015). Multiscale entropy analysis of biological signals: a fundamental bi-scaling law. *Front Comput Neurosci, 9*, 64. doi:10.3389/fncom.2015.00064

Grandy, T. H., Garrett, D. D., Schmiedek, F., & Werkle-Bergner, M. (2016). On the estimation of brain signal entropy from sparse neuroimaging data. *Scientific Reports, 6*. doi:10.1038/srep23073

Hadoush, H., Alafeef, M., & Abdulhay, E. (2019). Brain Complexity in Children with Mild and Severe Autism Spectrum Disorders: Analysis of Multiscale Entropy in EEG. *Brain Topogr*. doi:10.1007/s10548-019-00711-1

Harati, S., Crowell, A., Huang, Y., Mayberg, H., & Nemati, S. (2019). Classifying Depression Severity in Recovery from Major Depressive Disorder via Dynamic Facial Features. *IEEE J Biomed Health Inform*. doi:10.1109/jbhi.2019.2930604

Harati, S., Crowell, A., Mayberg, H., Jun, K., & Nemati, S. (2016). Discriminating clinical phases of recovery from major depressive disorder using the dynamics of facial expression. *Conf Proc IEEE Eng Med Biol Soc, 2016*, 2254-2257. doi:10.1109/embc.2016.7591178

Hasegawa, C., Takahashi, T., Yoshimura, Y., Nobukawa, S., Ikeda, T., Saito, D. N., . . . Kikuchi, M. (2018). Developmental Trajectory of Infant Brain Signal Variability: A Longitudinal Pilot Study. *Front Neurosci, 12*, 566. doi:10.3389/fnins.2018.00566

Heisz, J. J., & McIntosh, A. R. (2013). Applications of EEG Neuroimaging Data: Event-related Potentials, Spectral Power, and Multiscale Entropy. *Jove-Journal of Visualized Experiments*(76). doi:10.3791/50131

Heisz, J. J., Shedden, J. M., & McIntosh, A. R. (2012). Relating brain signal variability to knowledge representation. *Neuroimage, 63*(3), 1384-1392. doi:10.1016/j.neuroimage.2012.08.018

Heunis, T. M., Aldrich, C., & de Vries, P. J. (2016). Recent Advances in Resting-State Electroencephalography Biomarkers for Autism Spectrum Disorder-A Review of Methodological and Clinical Challenges. *Pediatr Neurol, 61*, 28-37. doi:10.1016/j.pediatrneurol.2016.03.010

Hier, D. B., Jao, C. S., & Brint, S. U. (1994). The Mental Status Expert (MSE): an expert system for scoring and interpreting the mental status examination. *Proc Annu Symp Comput Appl Med Care*, 1053.

Hu, M., & Liang, H. (2012). Adaptive multiscale entropy analysis of multivariate neural data. *IEEE Trans Biomed Eng, 59*(1), 12-15. doi:10.1109/tbme.2011.2162511

Hussain, L., Aziz, W., Saeed, S., Shah, S. A., Nadeem, M. S. A., Awan, I. A., . . . Kazmi, S. Z. H. (2018). Quantifying the dynamics of electroencephalographic (EEG) signals to distinguish alcoholic and non-alcoholic subjects using an MSE based K-d tree algorithm. *Biomed Tech (Berl), 63*(4), 481-490. doi:10.1515/bmt-2017-0041

Hussain, L., Saeed, S., Awan, I. A., & Idris, A. (2018). Multiscaled Complexity Analysis of EEG Epileptic Seizure Using Entropy-Based Techniques. *Archives of Neuroscience, 5*(1). doi:10.5812/archneurosci.61161

Jaworska, N., Wang, H., Smith, D. M., Blier, P., Knott, V., & Protzner, A. B. (2018). Pre-treatment EEG signal variability is associated with treatment success in depression. *Neuroimage Clin, 17*, 368-377. doi:10.1016/j.nicl.2017.10.035

Kaur, Y., Ouyang, G., Junge, M., Sommer, W., Liu, M., Zhou, C., & Hildebrandt, A. (2019). The reliability and psychometric structure of Multi-Scale Entropy measured from EEG signals at rest and during face and object recognition tasks. *J Neurosci Methods, 326*, 108343. doi:10.1016/j.jneumeth.2019.108343

Kielar, A., Deschamps, T., Chu, R. K., Jokel, R., Khatamian, Y. B., Chen, J. J., & Meltzer, J. A. (2016). Identifying Dysfunctional Cortex: Dissociable Effects of Stroke and Aging on Resting State Dynamics in MEG and fMRI. *Front Aging Neurosci, 8*, 40. doi:10.3389/fnagi.2016.00040

Kuntzelman, K., Jack Rhodes, L., Harrington, L. N., & Miskovic, V. (2018). A practical comparison of algorithms for the measurement of multiscale entropy in neural time series data. *Brain Cogn, 123*, 126-135. doi:10.1016/j.bandc.2018.03.010

Li, C. X., Chen, Y. N., Li, Y. J., Wang, J., & Liu, T. (2016). Complexity analysis of brain activity in attention-deficit/hyperactivity disorder: A multiscale entropy analysis. *Brain Research Bulletin, 124*, 12-20. doi:10.1016/j.brainresbull.2016.03.007

Lin, C., Lee, S. H., Huang, C. M., Chen, G. Y., Ho, P. S., Liu, H. L., . . . Wu, S. C. (2019). Increased brain entropy of resting-state fMRI mediates the relationship between depression severity and mental health-related quality of life in late-life depressed elderly. *J Affect Disord, 250*, 270-277. doi:10.1016/j.jad.2019.03.012

Liu, H., Yang, Z., Meng, F., Guan, Y., Ma, Y., Liang, S., . . . Li, L. (2017). Impairment of heart rhythm complexity in patients with drug-resistant epilepsy: An assessment with multiscale entropy analysis. *Epilepsy Research, 138*, 11-17. doi:10.1016/j.eplepsyres.2017.10.002

Liu, H., Yang, Z., Meng, F., Huang, L., Qu, W., Hao, H., . . . Li, L. (2018). Chronic vagus nerve stimulation reverses heart rhythm complexity in patients with drug-resistant epilepsy: An assessment with multiscale entropy analysis. *Epilepsy Behav, 83*, 168-174. doi:10.1016/j.yebeh.2018.03.035

Liu, H. Y., Yang, Z., Meng, F. G., Guan, Y. G., Ma, Y. S., Liang, S. L., . . . Li, L. M. (2018). Preoperative Heart Rate Variability as Predictors of Vagus Nerve Stimulation Outcome in Patients with Drug-resistant Epilepsy. *Sci Rep, 8*(1), 3856. doi:10.1038/s41598-018-21669-3

Liu, M., Song, C., Liang, Y., Knopfel, T., & Zhou, C. (2019). Assessing spatiotemporal variability of brain spontaneous activity by multiscale entropy and functional connectivity. *Neuroimage, 198*, 198-220. doi:10.1016/j.neuroimage.2019.05.022

Liu, Q., Chen, Y. F., Fan, S. Z., Abbod, M. F., & Shieh, J. S. (2015). EEG Signals Analysis Using Multiscale Entropy for Depth of Anesthesia Monitoring during Surgery through Artificial Neural Networks. *Computational and Mathematical Methods in Medicine*. doi:10.1155/2015/232381

Liu, Q., Chen, Y. F., Fan, S. Z., Abbod, M. F., & Shieh, J. S. (2017). EEG artifacts reduction by multivariate empirical mode decomposition and multiscale entropy for monitoring depth of anaesthesia during surgery. *Medical & Biological Engineering & Computing, 55*(8), 1435-1450. doi:10.1007/s11517-016-1598-2

Lu, W. Y., Chen, J. Y., Chang, C. F., Weng, W. C., Lee, W. T., & Shieh, J. S. (2015). Multiscale Entropy of Electroencephalogram as a Potential Predictor for the Prognosis of Neonatal Seizures. *Plos One, 10*(12). doi:10.1371/journal.pone.0144732

McIntosh, A. R., Kovacevic, N., & Itier, R. J. (2008). Increased Brain Signal Variability Accompanies Lower Behavioral Variability in Development. *Plos Computational Biology, 4*(7). doi:10.1371/journal.pcbi.1000106

McIntosh, A. R., Vakorin, V., Kovacevic, N., Wang, H., Diaconescu, A., & Protzner, A. B. (2014). Spatiotemporal Dependency of Age-Related Changes in Brain Signal Variability. *Cerebral Cortex, 24*(7), 1806-1817. doi:10.1093/cercor/bht030

Misic, B., Doesburg, S. M., Fatima, Z., Vidal, J., Vakorin, V. A., Taylor, M. J., & McIntosh, A. R. (2015). Coordinated Information Generation and Mental Flexibility: Large-Scale Network Disruption in Children with Autism. *Cerebral Cortex, 25*(9), 2815-2827. doi:10.1093/cercor/bhu082

Misic, B., Vakorin, V. A., Paus, T., & McIntosh, A. R. (2011). Functional embedding predicts the variability of neural activity. *Frontiers in Systems Neuroscience, 5*, 90. doi:10.3389/fnsys.2011.00090

Miskovic, V., Owens, M., Kuntzelman, K., & Gibb, B. E. (2016). Charting moment-to-moment brain signal variability from early to late childhood. *Cortex, 83*, 51-61. doi:10.1016/j.cortex.2016.07.006

Mizuno, T., Takahashi, T., Cho, R. Y., Kikuchi, M., Murata, T., Takahashi, K., & Wada, Y. (2010). Assessment of EEG dynamical complexity in Alzheimer's disease using multiscale entropy. *Clinical Neurophysiology, 121*(9), 1438-1446. doi:10.1016/j.clinph.2010.03.025

Nazari, A., Alavimajd, H., Shakeri, N., Bakhshandeh, M., Faghihzadeh, E., & Marzbani, H. (2019). Prediction of Brain Connectivity Map in Resting-State fMRI Data Using Shrinkage Estimator. *Basic Clin Neurosci, 10*(2), 147-156. doi:10.32598/bcn.9.10.140

Ouyang, G. X., Li, J., Liu, X. Z., & Li, X. L. (2013). Dynamic characteristics of absence EEG recordings with multiscale permutation entropy analysis. *Epilepsy Research, 104*(3), 246-252. doi:10.1016/j.eplepsyres.2012.11.003

Park, J. H., Kim, S., Kim, C. H., Cichocki, A., & Kim, K. (2007). Multiscale entropy analysis of EEG from patients under different pathological conditions. *Fractals-Complex Geometry Patterns and Scaling in Nature and Society, 15*(4), 399-404. doi:10.1142/S0218348x07003691

Puce, A., Berkovic, S. F., Cadusch, P. J., & Bladin, P. F. (1994). P3 latency jitter assessed using 2 techniques. I. Simulated data and surface recordings in normal subjects. *Electroencephalogr Clin Neurophysiol, 92*(4), 352-364. doi:10.1016/0168-5597(94)90103-1

Raja Beharelle, A., Kovacevic, N., McIntosh, A. R., & Levine, B. (2012). Brain signal variability relates to stability of behavior after recovery from diffuse brain injury. *Neuroimage, 60*(2), 1528-1537. doi:10.1016/j.neuroimage.2012.01.037

Richman, J. S., & Moorman, J. R. (2000). Physiological time-series analysis using approximate entropy and sample entropy. *American Journal of Physiology-Heart and Circulatory Physiology, 278*(6), H2039-H2049.

Riedl, M., Muller, A., & Wessel, N. (2013). Practical considerations of permutation entropy. *European Physical Journal-Special Topics, 222*(2), 249-262. doi:10.1140/epjst/e2013-01862-7

Roldan, E. M., Molina-Pico, A., Cuesta-Frau, D., Martinez, P. M., & Crespo, S. O. (2011). Characterization of entropy measures against data loss: application to EEG records. *Conf Proc IEEE Eng Med Biol Soc, 2011*, 6110-6113. doi:10.1109/iembs.2011.6091509

Sinai, M., Phillips, N. A., Chertkow, H., & Kabani, N. J. (2010). Task switching performance reveals heterogeneity amongst patients with mild cognitive impairment. *Neuropsychology, 24*(6), 757-774. doi:10.1037/a0020314

Sleimen-Malkoun, R., Perdikis, D., Muller, V., Blanc, J. L., Huys, R., Temprado, J. J., & Jirsa, V. K. (2015). Brain Dynamics of Aging: Multiscale Variability of EEG Signals at Rest and during an Auditory Oddball Task(1,2,3). *Eneuro, 2*(3). doi:10.1523/ENEURO.0067-14.2015

Szostakiwskyj, J. M. H., Willatt, S. E., Cortese, F., & Protzner, A. B. (2017). The modulation of EEG variability between internally-and externally-driven cognitive states varies with maturation and task performance. *Plos One, 12*(7). doi:10.1371/journal.pone.0181894

Takahashi, T., Cho, R., Mizuno, T., Kikuchi, M., Murata, T., Takahashi, K., & Wada, Y. (2010). Antipsychotics reverse abnormal EEG complexity in drug-naive schizophrenia: A multiscale entropy analysis. *International Journal of Neuropsychopharmacology, 13*, 242-243.

Takahashi, T., Cho, R. Y., Murata, T., Mizuno, T., Kikuchi, M., Mizukami, K., . . . Wada, Y. (2009). Age-related variation in EEG complexity to photic stimulation: A multiscale entropy analysis. *Clinical Neurophysiology, 120*(3), 476-483. doi:10.1016/j.clinph.2008.12.043

Takahashi, T., Yoshimura, Y., Hiraishi, H., Hasegawa, C., Munesue, T., Higashida, H., . . . Kikuchi, M. (2016). Enhanced brain signal variability in children with autism spectrum disorder during early childhood. *Human Brain Mapping, 37*(3), 1038-1050. doi:10.1002/hbm.23089

Ueno, K., Takahashi, T., Takahashi, K., Mizukami, K., Tanaka, Y., & Wada, Y. (2015). Neurophysiological basis of creativity in healthy elderly people: A multiscale entropy approach. *Clinical Neurophysiology, 126*(3), 524-531. doi:10.1016/j.clinph.2014.06.032

Valencia, J. F., Porta, A., Vallverdu, M., Claria, F., Baranowski, R., Orlowska-Baranowska, E., & Caminal, P. (2009). Refined Multiscale Entropy: Application to 24-h Holter Recordings of Heart Period Variability in Healthy and Aortic Stenosis Subjects. *Ieee Transactions on Biomedical Engineering, 56*(9), 2202-2213. doi:10.1109/Tbme.2009.2021986

Verhaeghe, J., Gravel, P., & Reader, A. J. (2010). Task-oriented quantitative image reconstruction in emission tomography for single- and multi-subject studies. *Phys Med Biol, 55*(23), 7263-7285. doi:10.1088/0031-9155/55/23/006

Wang, H., Pexman, P. M., Turner, G., Cortese, F., & Protzner, A. B. (2018). The relation between Scrabble expertise and brain aging as measured with EEG brain signal variability. *Neurobiology of Aging, 69*, 249-260. doi:10.1016/j.neurobiolaging.2018.05.015

Wang, H. Y., McIntosh, A. R., Kovacevic, N., Karachalios, M., & Protzner, A. B. (2016). Age-related Multiscale Changes in Brain Signal Variability in Pre-task versus Post-task Resting-state EEG. *Journal of Cognitive Neuroscience, 28*(7), 971-984. doi:10.1162/jocn_a_00947

Wei, Q., Li, Y., Fan, S. Z., Liu, Q., Abbod, M. F., Lu, C. W., . . . Shieh, J. S. (2014). A critical care monitoring system for depth of anaesthesia analysis based on entropy analysis and physiological information database. *Australasian Physical & Engineering Sciences in Medicine, 37*(3), 591-605. doi:10.1007/s13246-014-0285-6

Weng, W. C., Jiang, G. J., Chang, C. F., Lu, W. Y., Lin, C. Y., Lee, W. T., & Shieh, J. S. (2015). Complexity of Multi-Channel Electroencephalogram Signal Analysis in Childhood Absence Epilepsy. *Plos One, 10*(8), e0134083. doi:10.1371/journal.pone.0134083

Xu, Y., Cui, J., Hong, W., & Liang, H. (2015). [Automatic Classification of Epileptic Electroencephalogram Signal Based on Improved Multivariate Multiscale Entropy]. *Sheng Wu Yi Xue Gong Cheng Xue Za Zhi, 32*(2), 256-262.

Yang, A. C., Wang, S. J., Lai, K. L., Tsai, C. F., Yang, C. H., Hwang, J. P., . . . Fuh, J. L. (2013). Cognitive and neuropsychiatric correlates of EEG dynamic complexity in patients with Alzheimer's disease. *Progress in Neuro-Psychopharmacology & Biological Psychiatry, 47*, 52-61. doi:10.1016/j.pnpbp.2013.07.022

Zanin, M., Zunino, L., Rosso, O. A., & Papo, D. (2012). Permutation Entropy and Its Main Biomedical and Econophysics Applications: A Review. *Entropy, 14*(8), 1553-1577. doi:10.3390/e14081553

Zavala-Yoe, R., Ramirez-Mendoza, R., & Cordero, L. M. (2015). Novel way to investigate evolution of children refractory epilepsy by complexity metrics in massive information. *Springerplus, 4*. doi:10.1186/s40064-015-1173-6